ARTICLE

doi:10.1038/nature16193

DDX5 and its associated lncRNA *Rmrp* modulate T_H17 cell effector functions

Wendy Huang[1], Benjamin Thomas[2], Ryan A. Flynn[3], Samuel J. Gavzy[1], Lin Wu[1], Sangwon V. Kim[1], Jason A. Hall[1], Emily R. Miraldi[1,4,5,6], Charles P. Ng[1], Frank Rigo[7], Sarah Meadows[8], Nina R. Montoya[1], Natalia G. Herrera[1], Ana I. Domingos[9], Fraydoon Rastinejad[10], Richard M. Myers[8], Frances V. Fuller-Pace[11], Richard Bonneau[4,5,6], Howard Y. Chang[3], Oreste Acuto[2] & Dan R. Littman[1,12]

T helper 17 (T_H17) lymphocytes protect mucosal barriers from infections, but also contribute to multiple chronic inflammatory diseases. Their differentiation is controlled by RORγt, a ligand-regulated nuclear receptor. Here we identify the RNA helicase DEAD-box protein 5 (DDX5) as a RORγt partner that coordinates transcription of selective T_H17 genes, and is required for T_H17-mediated inflammatory pathologies. Surprisingly, the ability of DDX5 to interact with RORγt and coactivate its targets depends on intrinsic RNA helicase activity and binding of a conserved nuclear long noncoding RNA (lncRNA), *Rmrp*, which is mutated in patients with cartilage-hair hypoplasia. A targeted *Rmrp* gene mutation in mice, corresponding to a gene mutation in cartilage-hair hypoplasia patients, altered lncRNA chromatin occupancy, and reduced the DDX5–RORγt interaction and RORγt target gene transcription. Elucidation of the link between *Rmrp* and the DDX5–RORγt complex reveals a role for RNA helicases and lncRNAs in tissue-specific transcriptional regulation, and provides new opportunities for therapeutic intervention in T_H17-dependent diseases.

T_H17 cells are $CD4^+$ lymphocytes that help to protect mucosal epithelial barriers against bacterial and fungal infections[1], and are also important in multiple autoimmune diseases[2–7]. The T_H17 cell differentiation program is defined by the induced expression of RORγt (ref. 2), a sterol ligand-regulated nuclear receptor that focuses the activity of a cytokine-regulated transcriptional network upon a subset of key genomic target sites, including genes encoding the signature T_H17 cytokines (interleukin (IL)-17A, IL-17F and IL-22) as well as IL-23R, IL-1R1 and CCR6 (ref. 8). In mouse models, attenuation of RORγt activity results in protection from experimental autoimmune encephalomyelitis (EAE), T-cell-transfer-mediated colitis and collagen-induced arthritis[2–5]. Like other nuclear receptors, RORγt interaction with its ligands results in recruitment of coactivators at regulated genomic loci[9]. We identified two new RORγt partners in T_H17 cells, an RNA helicase and a lncRNA, which together associate with RORγt to confer target-locus-specific activity in enabling the T-cell effector program.

The RNA helicase DDX5 functions in multiple cellular processes[10], including transcription and ribosome biogenesis[11–17], in both a helicase-activity-dependent and -independent manner. The lncRNA *Rmrp*, RNA component of mitochondria RNA processing endoribonuclease (also known as RNase MRP), is highly conserved between mouse and human and is essential for early mouse development[18]. *Rmrp* was first identified as a component of the RNase MRP complex that cleaves mitochondrial RNAs[19]. In yeast, the *RMRP1* gene contributes to ribosomal RNA processing and regulates messenger RNA (mRNA) degradation[20]. In humans, mutations located in evolutionarily conserved nucleotides at the promoter or within the transcribed region of *RMRP* result in cartilage-hair hypoplasia (CHH), a rare autosomal recessive disorder characterized by early childhood onset of skeletal dysplasia, hypoplastic hair, defective immunity, predisposition to lymphoma and neuronal dysplasia of the intestine[21,22]. Immune deficiency in CHH patients is associated with recurrent infections, haematological abnormalities and autoimmune pathologies in the joints and kidneys[23]. The precise mechanisms by which *Rmrp* functions in the immune system have yet to be determined. Here we show that the helicase activity of DDX5 mediates *Rmrp*-dependent binding to RORγt and recruitment to a subset of chromatin target sites, thus controlling the differentiation of T_H17 cells at steady state and in animal models of autoimmunity.

DDX5 regulation of RORγt target genes

To identify novel interacting partners of RORγt in T_H17 cells, we enriched for endogenous RORγt-containing protein complexes and subsequently determined protein composition using liquid-chromatography–tandem mass spectroscopy (LC–MS/MS) (workflow shown in Extended Data Fig. 1a). Among the top hits of RORγt-interacting proteins was the RNA helicase DDX5. We validated this interaction through conventional co-immunoprecipitation experiments followed by immunoblot analysis (Extended Data Fig. 1b).

We investigated the function of DDX5 in T cells by breeding *Ddx5* conditional mutant mice with CD4-Cre mice to generate T-cell-specific DDX5-deficient mice ($Ddx5^{fl/fl}$ CD4-Cre mice, denoted DDX5-T). DDX5-T mice were born at the expected Mendelian ratio, were fertile, and did not display any gross phenotypic abnormalities. The activation status of T cells in the periphery was similar between $Ddx5^{+/+}$ CD4-Cre^+ (wild type) and mutant mice (Extended Data Fig. 1c) that had no DDX5 protein in spleen and lymph node $CD4^+$ T cells (Extended Data Fig. 1d). Naive $CD4^+$ T cells sorted from wild-type and DDX5-T mice did not display differences in polarization towards

[1]The Kimmel Center for Biology and Medicine of the Skirball Institute, New York University School of Medicine, New York, New York 10016, USA. [2]Sir William Dunn School of Pathology, University of Oxford, Oxford OX1 3RE, UK. [3]Center for Personal Dynamic Regulomes, Stanford University, Stanford, California 94305, USA. [4]Center for Genomics and Systems Biology, Department of Biology, New York University, New York, New York 10003, USA. [5]Courant Institute of Mathematical Sciences, Computer Science Department, New York University, New York, New York 10012, USA. [6]Simons Center for Data Analysis, Simons Foundation, New York, New York 10010, USA. [7]Isis Pharmaceuticals, Carlsbad, California 92010, USA. [8]HudsonAlpha Institute for Biotechnology, Huntsville, Alabama 35806, USA. [9]Instituto Gulbenkian de Ciencia, Oeiras 2780-156, Portugal. [10]Integrative Metabolism Program, Sanford Burnham Prebys Medical Discovery Institute, Orlando, Florida 32827, USA. [11]Division of Cancer Research, University of Dundee, Dundee DD1 9SY, UK. [12]Howard Hughes Medical Institute, New York University School of Medicine, New York, New York 10016, USA.

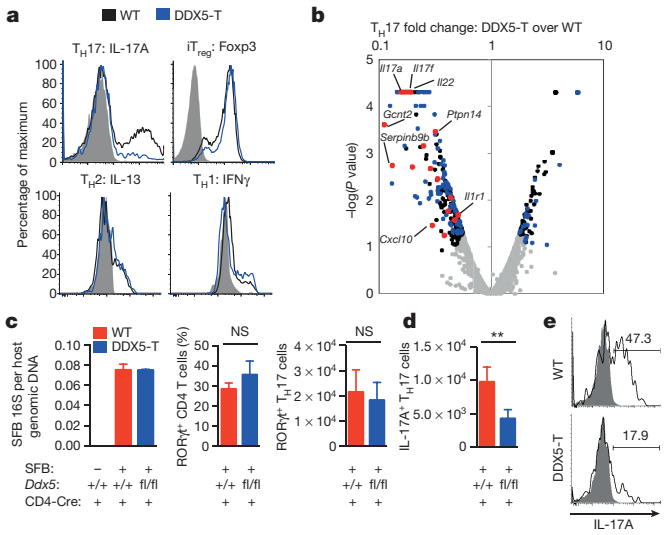

Figure 1 | Requirement for DDX5 in T_H17 cytokine production *in vitro* and at steady state *in vivo*. **a**, Selective T_H17 cell differentiation defect in DDX5-deficient T cells (DDX5-T) after polarization for 96 h. Representative of three independent experiments. WT, wild type. **b**, Volcano plot of RNA-seq of cultured T_H17 cells from DDX5-T mice and littermate controls. Black dots, differentially expressed genes (minimum fold change of two with $P < 0.05$). Blue dots, known RORγt-dependent genes. Red dots, top RORγt–DDX5-coregulated genes. **c**, **d**, SFB colonization and percentage and number of RORγt$^+$CD4$^+$ T cells (**c**) and number of IL-17A-producing CD4$^+$ T cells (**d**) in ileal lamina propria of co-housed wild-type (+/+; $n = 5$) and DDX5-T (fl/fl; $n = 5$) CD4-Cre$^+$ mice. Graphs show mean ± s.d. from two independent experiments, combined. NS, not significant. $^{**}P < 0.01$ (paired *t*-test). **e**, Representative IL-17A expression in CD4$^+$Foxp3$^-$RORγt$^+$ T_H17 cells from ileal lamina propria of wild-type and DDX5-T mice after restimulation.

T_H1, T_H2 and induced regulatory T (iT_{reg}) cell phenotypes *in vitro* (Fig. 1a). In contrast, DDX5-T naive T cells cultured under T_H17-polarizing conditions produced substantially less IL-17A than wild-type cells (Fig. 1a). RORγt protein expression and nuclear localization were similar between wild-type and DDX5-T T_H17-polarized cells (Extended Data Fig. 1d, e), and, like RORγt, DDX5 protein localized mainly to the nucleus (Extended Data Fig. 1f). These results suggest that DDX5 is not required for T_H17 lineage commitment, but contributes to T_H17 cell effector functions.

DDX5 can function as a transcriptional coactivator[12,24,25], augmenting the activities of other nuclear receptor family members, including the oestrogen and androgen receptors[12,26]. To determine whether DDX5 partners with RORγt to facilitate the T_H17 cell transcriptional program, we performed RNA sequencing (RNA-seq) on *in vitro* polarized T_H17 cells from wild-type or DDX5-T mice. Among the 325 genes that were significantly dysregulated in DDX5-deficient T cells 96 h after polarization, approximately 40% had been previously identified as RORγt targets in T_H17 cells[8] (Extended Data Fig. 2a). Ingenuity Pathway Analysis (Qiagen) of DDX5–RORγt-coregulated genes revealed enrichment in 'T helper cell differentiation program' as well as 'interleukin production' (Extended Data Fig. 2b). Coregulated genes (Fig. 1b) included those for the signature T_H17 cytokines (*Il17a*, *Il17f* and *Il22*) (Extended Data Fig. 2c). Independent biological samples were used to validate a subset of RORγt target genes with and without altered expression in DDX5-deficient T_H17 cells (Extended Data Fig. 2d).

We used anti-DDX5 antibodies in genome-wide chromatin immunoprecipitation sequencing (ChIP-seq) studies to identify DDX5-occupied loci. A specific subset of previously published RORγt-occupied loci, including *Il17a* and *Il17f*, were enriched for DDX5 co-localization, as determined by seqMINER clustering analysis (Extended Data Fig. 3a, b). ChIP with quantitative PCR (ChIP-qPCR) was used to validate DDX5 enrichment at the *Il17a* and *Il17f* loci and its dependency on RORγt in polarized T_H17 cells (Extended Data Fig. 3c). These results suggest that DDX5 overlaps with RORγt in modulating a specific subset of the T_H17 cell transcriptional program.

DDX5 function *in vivo* in T_H17 cells

At steady state, cytokine-producing T_H17 cells populate the small intestinal lamina propria of animals colonized with commensal segmented filamentous bacteria (SFB)[27]. When colonized with SFB, DDX5-T mice and wild-type littermates had similar numbers of ileal-residing Foxp3$^-$RORγt$^+$CD4$^+$ T_H17 cells (Fig. 1c). However, the number and proportion of IL-17A-producing cells among RORγt$^+$CD4$^+$ cells from DDX5-T mice were markedly reduced compared to wild-type littermate controls (Fig. 1d, e).

To evaluate the role of DDX5 in T_H17-driven inflammation, we used a T-cell transfer model of colitis, in which disease severity is dependent on RORγt expression in donor T cells[3,28]. Following transfer of CD4$^+$CD45RB^{hi} T cells into Rag-deficient (*Rag2*$^{-/-}$) recipients, mice that received wild-type T cells experienced weight loss (Fig. 2a) and developed colitis (Fig. 2b), whereas recipients of DDX5-T cells did not. Total RNA from large intestine lamina propria mononuclear cells revealed a significant reduction of both *Il17a* and *Ifng* transcripts from recipients of DDX5-T cells compared to wild-type controls (Extended Data Fig. 4a). Interestingly, there were comparable proportions of IFNγ-producing CD4$^+$RORγt$^-$T-bet$^+$ (conventional T_H1) cells in recipients of T cells from either wild-type or DDX5-T mice (Extended Data Fig. 4b). However, recipients of cells from DDX5-T mice displayed a significant reduction in CD4$^+$Foxp3$^-$RORγt$^+$ T cells co-expressing IL-17A and IFNγ, an important feature of pathogenic T cells in several inflammatory disease settings[2,29,30] (Fig. 2c and

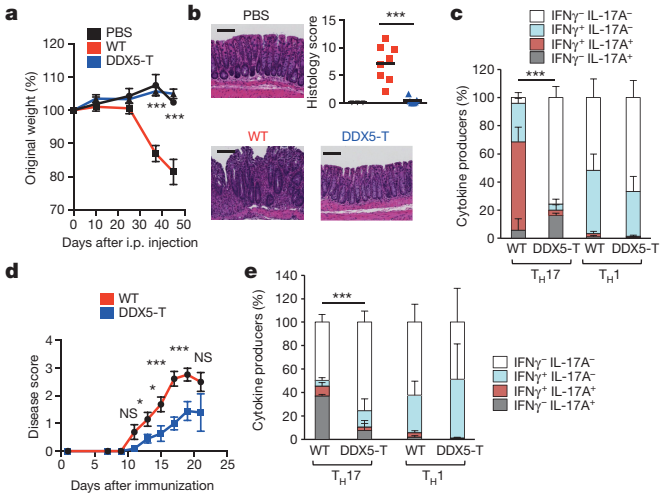

Figure 2 | Role of DDX5 in mouse models of T_H17-cell-mediated autoimmune disease. **a**, Weight change in *Rag2*$^{-/-}$ recipients of wild-type or DDX5-T CD4$^+$ naive T cells in the transfer model of colitis measured on days 0, 10, 25, 37 and 45 (PBS, $n = 4$; wild type, $n = 9$; DDX5-T, $n = 13$, combined from three independent experiments). i.p., intraperitoneal. **b**, Haematoxylin and eosin (H&E) staining and analysis of large intestine at day 45. Representative sections (scale bars, 100 μm) and histology scores (scale of 0–24) are shown. Scores for PBS ($n = 3$), wild-type (red, $n = 8$) and DDX5-T (blue, $n = 7$) mice are from two independent experiments. **c**, Cytokine production defect in DDX5-T T_H17 (RORγt$^+$) but not T_H1 (RORγt$^-$T-bet$^+$) cells in large intestine lamina propria at day 45 ($n = 4$ per group). **d**, EAE disease scores (scale of 0–5) in co-housed myelin oligodendrocyte glycoprotein (MOG)-immunized littermates. Wild-type ($n = 13$) and DDX5-T ($n = 11$) mice, combined from three independent experiments. **e**, Defective IL-17A production in DDX5-T CD4$^+$RORγt$^+$ cells in the spinal cord of MOG-immunized mice ($n = 7$ per group). Graphs show mean ± s.d. $^*P < 0.05$, $^{**}P < 0.01$; $^{***}P < 0.001$ (unpaired, *t*-test).

Extended Data Fig. 4b). Consistent with a loss of pathogenic capacity, DDX5-T mice also exhibited attenuated disease compared to wild-type controls during EAE (Fig. 2d). Analysis of spinal cord infiltrates after immunization revealed a reduced proportion of IL-17A-producing $CD4^+$ T cells (Fig. 2e and Extended Data Fig. 4c). Consistent with our *in vitro* findings, these results in mice indicate that DDX5 selectively regulates the T_H17 effector program, both in steady state and under inflammatory conditions.

Function of DDX5–associated lncRNA

RNA helicases are highly conserved enzymes that utilize the energy derived from ATP hydrolysis to unwind RNA duplexes, facilitate RNA annealing, and displace proteins from RNA. It was previously shown that DDX5 transcriptional coactivator activity for oestrogen receptor, androgen receptor and the transcription factor RUNX2 is independent of RNA helicase activity[12,24,26]. We tested this requirement in the context of RORγt by retroviral transduction of DDX5-deficient T cells cultured under T_H17-polarizing conditions with expression constructs for wild-type or mutant DDX5 with an inactivated helicase domain (helicase-dead). Surprisingly, only wild-type DDX5 rescued IL-17A and IL-17F production in these polarized T_H17 cells (Fig. 3a, b and Extended Data Fig. 5a). This result suggested that perhaps RNA substrate(s) for the helicase activity of DDX5 contribute to its transcriptional coactivator role in T_H17 cells.

We next searched for RNA molecules that might participate in DDX5–RORγt-mediated transcription in T_H17 cells. We first depleted ribosome-bound mRNAs undergoing active protein synthesis. Lysates pre-cleared of ribosomes were then subjected to RNA immunoprecipitation (RIP) with antibodies specific for DDX5 or RORγt, followed by deep sequencing of the associated RNAs (RIP-seq). Among 49,893 annotated lncRNAs in the mouse RefSeq and NONCODE database, 2,533 noncoding RNAs were expressed in T_H17 cells (fragments per kilobase of transcripts per million mapped reads (FPKM) >1, Extended Data Fig. 5b). Interestingly, the steroid receptor RNA activator (*SRA*) lncRNA, previously found to be associated with DDX5 in muscle cells[15], was not enriched in DDX5-containing protein complexes in T_H17 cells. Instead, we found *Rmrp* to be the most enriched RNA associated with DDX5 and, to a lesser degree, RORγt, in T_H17 cells (Fig. 3c and Extended Data Fig. 5c). RIP-qPCR with independent biological samples confirmed enrichment of *Rmrp* RNA in DDX5 pull-downs from T_H17 cells, but not from thymocyte lysates (Extended Data Fig. 5d).

RNA fluorescence *in situ* hybridization revealed that *Rmrp* is localized in the nucleus of T_H17 cells (Extended Data Fig. 6a). To evaluate the functional role of *Rmrp*, we transiently depleted *Rmrp* RNA from primary mouse T_H17 cells using an RNaseH-dependent antisense oligonucleotide (ASO). Similar to the DDX5-deficient T_H17 cells, cells depleted of *Rmrp* expressed reduced *Il17a* and *Il17f* mRNA (Fig. 3d and Extended Data Fig. 6b). Human T_H17 cells also displayed reduced cytokine production upon depletion of *RMRP* or DDX5 (Fig. 3e and Extended Data Fig. 6c), suggesting that this regulatory mechanism is evolutionarily conserved. Notably, *Rmrp* RNA knockdown in DDX5-deficient mouse T_H17 cells did not further reduce IL-17A and IL-17F expression (Fig. 4a). Expression of RORγt-dependent, but DDX5-independent, CCR6 was unaffected by the reduction in *Rmrp*. Transduction of *Rmrp* into T cells cultured in T_H1-polarization conditions had little effect on IFNγ production, but there was marked enhancement of IL-17A and IL-17F production in wild-type, but not DDX5-deficient, cells cultured in T_H17-polarization conditions (Fig. 4b and Extended Data Fig. 7a, b). Thus, *Rmrp*-dependent cytokine gene expression requires the presence of DDX5.

T_H17 program in *Rmrp* mutant mice

In contrast to wild-type *Rmrp*, a mutant *Rmrp* carrying a single nucleotide change (270G > T), corresponding to an allele identified in CHH patients (262G > T), failed to potentiate IL-17A production

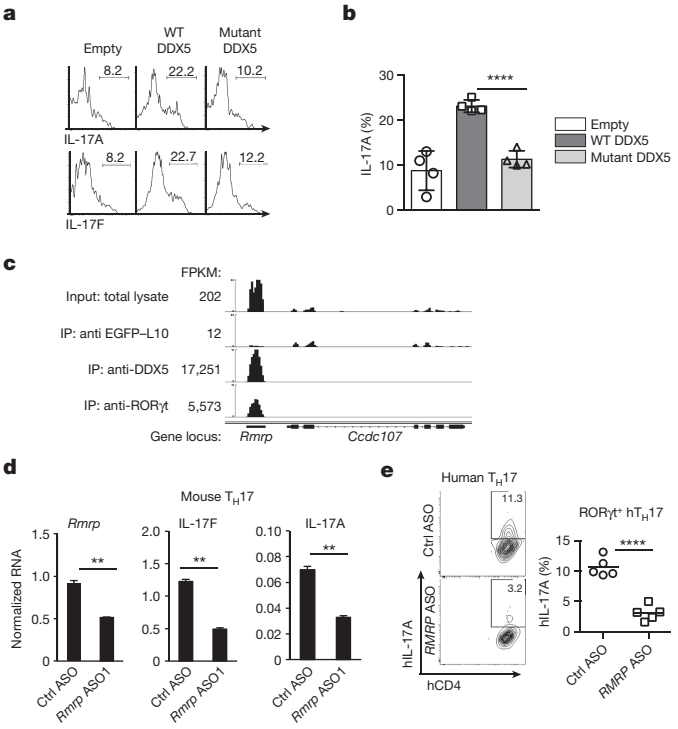

Figure 3 | Requirement for helicase-competent DDX5 and its associated lncRNA *Rmrp* in induction of T_H17 cell cytokines. a, **b**, Cytokine production in DDX5-T cells transduced with wild-type or helicase-mutant DDX5 and subjected to sub-optimal T_H17 cell polarization. Results from four independent experiments shown. **c**, IGV browser view of *Rmrp* showing coverage of mapped RNA reads from total T_H17 lysate, ribosome TRAP-seq (EGFP-L10; described in Methods), DDX5 RIP-seq and RORγt RIP-seq. IP, immunoprecipitate. **d**, Effect of mouse *Rmrp*-specific ASO. Results are representative of three independent experiments with two technical replicates. Ctrl, control. **e**, IL-17A production following *RMRP* knockdown in *in vitro* polarized human T_H17 cells. Each data point (right panel) represents cells from a healthy donor ($n = 5$). Graphs show mean ± s.d. $^{**}P < 0.01$; $^{****}P < 0.0001$ (unpaired, *t*-test).

after transduction into T_H17-polarized cells (Extended Data Fig. 7c, d). To investigate whether G270 of *Rmrp* contributes to RORγt transcriptional output *in vivo*, we generated mice homozygous for the *Rmrp* G270T point mutation, using CRISPR-Cas9 (clustered, regularly interspaced short palindromic repeats coupled with CRISPR-associated proteins) technology (Fig. 4c). The mice were born at the expected Mendelian ratios and had no gross defects. ROR response element (RORE)-regulated luciferase activity was reduced in transiently transfected T_H17 cells from DDX5-deficient and $Rmrp^{G270T}$ mice and after ASO-mediated knockdown of *Rmrp* (Fig. 4d). Comparison of the transcription profiles of *in vitro* polarized T_H17 cells from wild-type, RORγt-deficient, DDX5-deficient and $Rmrp^{G270T/G270T}$ mice indicated that 96 RORγt-dependent T_H17 cell genes were coregulated by *Rmrp* together with DDX5 (Extended Data Fig. 7e and Fig. 4e). Reverse transcription (RT)–qPCR analysis of independent biological samples from *in vitro* polarized T cells from wild-type and $Rmrp^{G270T/G270T}$ mice confirmed reduced *Il17f* mRNA expression in the latter (Extended Data Fig. 7f), despite a similar amount of RORγt binding to known *cis*-regulatory loci (Extended Data Fig. 7g). The proportion of $ROR\gamma t^+Foxp3^-$ T_H17 cells among total ileal lamina propria CD4-lineage cells was unaffected in $Rmrp^{G270T/G270T}$ mice, but these cells expressed relatively little IL-17A compared to those in wild-type littermates (Fig. 4f). Transfer of $Rmrp^{G270T/G270T}$ T cells into $Rag2^{-/-}$ mice resulted in reduced colitis, as determined by weight loss and colon histology, compared to the transfer of wild-type cells (Extended Data Fig. 8a). These phenotypes are similar to those observed in recipients of DDX5-deficient T-cells

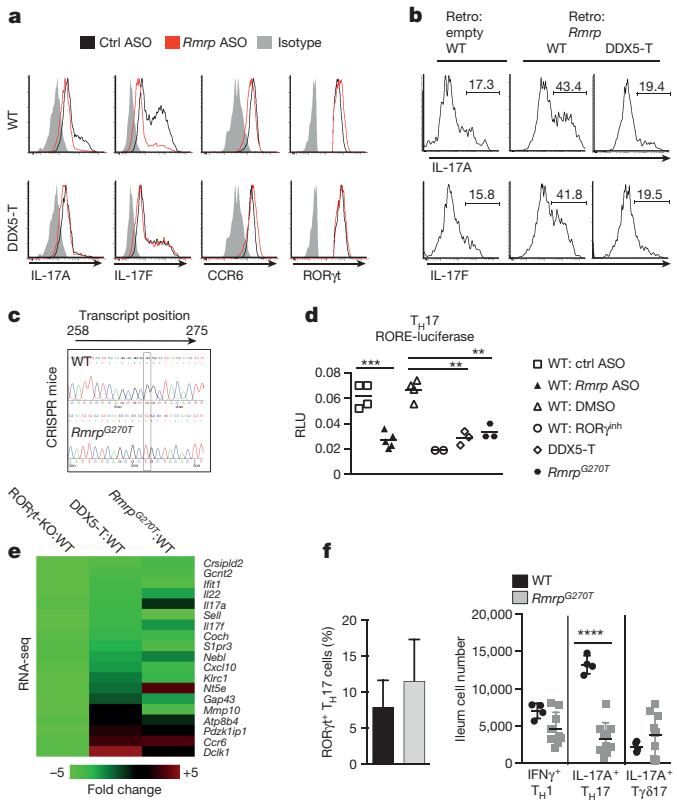

Figure 4 | Analysis of DDX5-dependent *Rmrp* function in T_H17 cell differentiation. a, **b**, Cytokines in wild-type and DDX5-T *in vitro* polarized T_H17 cells after *Rmrp* knockdown (**a**) or overexpression (**b**). Representative of three independent experiments. **c**, Sequence of the *Rmrp* gene (nucleotides 258–275) from wild-type and $Rmrp^{G270T/G270T}$ littermates. **d**, *Rmrp*-dependent expression of a RORE-directed firefly luciferase reporter nucleofected into polarized T_H17 cells at 72 h. Firefly and control *Renilla* luciferase activities were measured 24 h later. Each dot represents the result from one nucleofection. Results from two independent experiments. DMSO, dimethyl sulfoxide; RLU, relative luciferase units; $ROR\gamma^{inh}$, RORγ antagonist ML209. **e**, Top RORγt targets coregulated by DDX5 and *Rmrp*. **f**, Proportion of $CD4^+Foxp3^-$ T cells expressing RORγt (left) and numbers of T_H1 ($IFN\gamma^+ROR\gamma t^-Tbet^+$), T_H17 ($IL\text{-}17A^+ROR\gamma t^+Foxp3^-$) and Tγδ17 ($IL\text{-}17A^+T\gamma\delta^+ROR\gamma t^+$) cells (right) in small intestine lamina propria. Symbols represent cells from one mouse. Graphs show mean ± s.d. $^{**}P < 0.01$; $^{***}P < 0.001$; $^{****}P < 0.0001$ (unpaired, *t*-test).

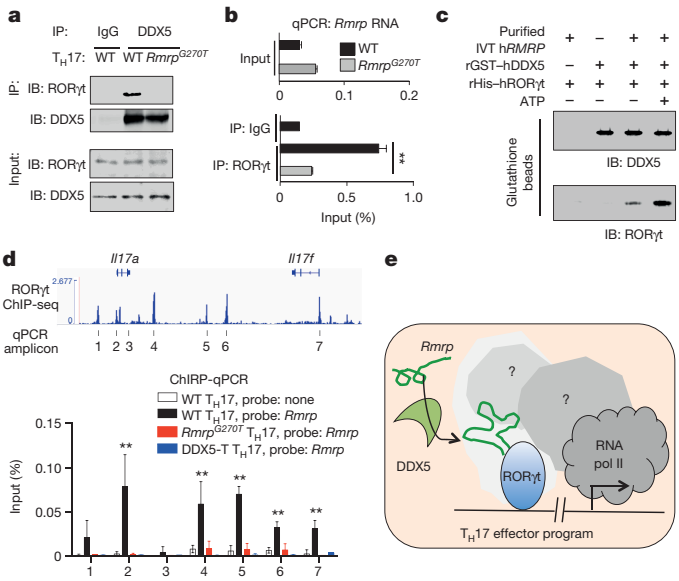

Figure 5 | *Rmrp* localization at RORγt-occupied genes and role in RORγt–DDX5 assembly. a, RORγt association with immunoprecipitated DDX5 in polarized T_H17 cells. IB, immunoblot. Representative of three independent experiments. **b**, *Rmrp* quantification by RT–qPCR in RORγt immunoprecipitates from polarized T_H17 cells. Representative of two independent experiments with two technical replicates. **c**, *Rmrp* requirement for ATP-dependent *in vitro* interaction of recombinant (r) glutathione *S*-transferase (GST)–DDX5 and His–RORγt. Representative of three independent experiments. IVT, *in vitro* transcribed RNA. For uncropped gels (**a**, **c**), see Supplementary Fig. 1. **d**, *Rmrp* occupancy at RORγt genomic target loci in polarized T_H17 cells. *Rmrp* ChIRP-qPCR amplicons (bottom) are indicated in IGV browser view of RORγt ChIP-seq at the *Il17* locus (top). Data from 2–4 experiments with two technical replicates. **e**, Model for DDX5–*Rmrp* complex recruitment to RORγt-occupied chromatin in T_H17 cells. Graphs show mean ± s.d. $^{**}P < 0.01$ (unpaired, *t*-test).

(Fig. 2a–c), which is consistent with an important role of *Rmrp* G270 in executing the T_H17 effector program *in vivo*.

RORγt and its closely related isoform RORγ perform distinct functions in diverse tissues. RORγt is critical for thymocyte development, regulating the survival of double-positive $CD4^+CD8^+$ cells, and development of secondary and tertiary lymphoid organs mediated by lymphoid tissue inducer cells[31]. While DDX5 and *Rmrp* are ubiquitously expressed, *Rmrp* was less enriched in thymocyte-derived than in T_H17-cell-derived DDX5 immunoprecipitates (Extended Data Fig. 5d). When *Ddx5* was inactivated at the common lymphoid progenitor stage, by breeding the conditional mutant mice with IL7R-Cre mice, there was no apparent defect in thymocyte subset development (Extended Data Fig. 8b). Similarly, $Rmrp^{G270T}$ knock-in mice displayed normal thymocyte subsets and also had intact secondary lymphoid organ development (Extended Data Fig. 8c). Together, these results suggest that the DDX5–*Rmrp* complex performs T_H17-specific functions.

Rmrp in DDX5–RORγt complex formation

We next investigated how *Rmrp* contributes to the DDX5–RORγt-regulated transcriptional circuit in T_H17 cells. RORγt–DDX5 complex assembly was severely compromised in T_H17 cells from $Rmrp^{G270T}$ mice (Fig. 5a). Moreover, *Rmrp* recruitment to the RORγt protein complex was significantly reduced in T_H17 cells from *Rmrp* mutant animals (Fig. 5b). *In vitro*, *Rmrp* binds directly to recombinant DDX5 (Extended Data Fig. 9a). Notably, *Rmrp* was recruited to RORγt in the presence of wild-type, but not helicase-dead, DDX5. Furthermore, *in vitro* transcribed *Rmrp* RNA promoted RORγt interaction with wild-type, but not helicase-dead, DDX5 in the presence of ATP (Fig. 5c and Extended Data Fig. 9b). Mutant *Rmrp* was also defective in mediating DDX5–RORγt complex assembly *in vitro* (Extended Data Fig. 9c, d).

To determine whether *Rmrp* is associated with specific genomic loci, we performed chromatin isolation by RNA purification (ChIRP) followed by either locus-specific qPCR or deep sequencing (ChIRP-seq)[32]. We used two orthogonal antisense probe sets that specifically and robustly recovered *Rmrp* from T_H17 cells (Extended Data Fig. 10a). When combined for *Rmrp* ChIRP-qPCR, the probes recovered RORγt-bound regions in the *Il17a* and *Il17f* loci from T_H17-polarized cells of wild-type but not DDX5-T or $Rmrp^{G270T/G270T}$ mice, in an RNase-sensitive manner (Fig. 5d and Extended Data Fig. 10b). For ChIRP-seq, we focused our analysis on signals that overlapped with separate use of the two probe sets. HOMER motif analyses of *Rmrp* peak regions identified the ETS, DR2/RORE and AP1 transcription factor motifs to be the most highly enriched (Extended Data Fig. 10c). Consistent with this, *Rmrp* ChIRP-seq significantly overlapped with RORγt-bound loci, but not with sites occupied by CTCF or by other T_H17 transcription factors, such as BATF, IRF4, STAT3 and c-Maf (Extended Data Fig. 10d). There was also significant overlap with RNA polymerase II (Pol II)- and histone H3 lysine 4 trimethylation (H3K4me3)-associated chromatin, which mark actively transcribed regions. Concordantly, ChIRP-seq of *Rmrp* in DDX5-T T_H17

cells revealed a loss of called *Rmrp* peaks (Extended Data Fig. 10e), consistent with a DDX5 contribution to *Rmrp* association with chromatin. *Rmrp* association with RORγt-bound sites was also reduced in polarized T_H17 cells from $Rmrp^{G270T/G270T}$ mice despite a similar amount of RNA recovery (Extended Data Fig. 10f). Together, these results indicate that G270 of *Rmrp* is critical for DDX5–RORγt complex assembly and *Rmrp* recruitment to RORγt-occupied loci to coordinate the T_H17 effector program in *trans*.

Discussion

Nuclear lncRNAs have key roles in numerous biological processes[33] including adaptive and innate immunity[34,35], but how individual lncRNAs perform their activities and whether they contribute to immunological diseases remain unknown. We identified nuclear *Rmrp* as a key DDX5-associated RNA required to promote assembly and regulate the function of RORγt transcriptional complexes at a subset of critical genes implicated specifically in the T_H17 effector program (model in Fig. 5e). *Rmrp* thus acts in *trans* on multiple RORγt-dependent genes, and does so only upon interaction with enzymatically active DDX5 helicase. RNA-helicase-dependent functions of lncRNAs have been described, for example, the *Drosophila* male cell-specific lncRNAs roX1 and roX2 that are modified by the MLE helicase to enable expression of X-chromosome genes[36,37]. In addition, DDX21 helicase activity in HEK293 cells is required for 7SK RNA regulation of polymerase pausing at ribosomal genes[38]. Our results extend the concept of RNA helicase/lncRNA function to lineage-specific regulation of transcriptional programs.

Notably, unlike most lncRNAs, *Rmrp* is highly conserved among mammals. In humans, mutations of evolutionarily conserved nucleotides at the promoter or within the transcribed region of *RMRP* result in CHH[21,22]. T cells from mice carrying a single nucleotide change (270G > T) in *Rmrp*, corresponding to one found in CHH patients (262G > T), had a compromised T_H17 cell effector program. CHH patients have been noted to have defective T-cell-dependent immunity, which may in part reflect reduced *RMRP*-dependent activity at RORγt target genes. As forced expression of either DDX5 or *Rmrp* enhanced T_H17 cytokine production, it is also possible that gain-of-function mutations in either of these molecules may contribute to T_H17-dependent inflammatory diseases.

RORγt is an attractive therapeutic target for multiple autoimmune diseases[5,39]. However, RORγt and RORγ have several other functions that would probably be affected by targeting of their shared ligand-binding pocket. RORγt is required for the development of early thymocytes, lymphoid tissue inducer cells that initiate lymphoid organogenesis[31], type 3 innate lymphoid cells that produce IL-22 and protect epithelial barriers, and for IL-17 production by 'innate-like' T cells, including T cell receptor (TCR)γδ and natural killer T cells[40–43]. In the liver, RORγ contributes to regulation of metabolic functions[44]. Mechanisms by which RORγt and RORγ differentially regulate transcription in these diverse cell types remain poorly understood. DDX5 and *Rmrp* are abundantly expressed in developing T cells in the thymus and in peripheral naive and differentiated T-helper subsets (W.H., unpublished observations). Notably, the contribution of DDX5–*Rmrp* to RORγt-dependent functions appears to be confined to T_H17 cells, as their loss of function did not affect thymocyte or lymphoid organ development. Our results raise the prospect that tissue- or cell-type-specific mechanisms exist to regulate how RNA helicases and their associated lncRNAs are assembled with distinct transcriptional complexes to promote diverse gene expression programs.

We speculate that the function of DDX5–*Rmrp* may be induced in response to specific tissue microenvironments *in vivo*. T_H17 cells differentiate at mucosal barriers in response to signals from the microbiota, and upregulate their expression of IL-17A locally[45,46]. Regional signals may induce DDX5/*Rmrp* association with RORγt, resulting in the transcriptional activation of multiple loci that enable T_H17 cell effector functions. Our finding that DDX5 was required for the differentiation of 'pathogenic' T_H17 cells[2,29,30] suggests that strategies to interfere with this function may be of therapeutic benefit. A better understanding of this transcriptional regulatory system may provide new approaches for therapeutic intervention in autoimmune diseases and immune deficiencies in CHH patients.

Online Content Methods, along with any additional Extended Data display items and Source Data, are available in the online version of the paper; references unique to these sections appear only in the online paper.

Received 18 June; accepted 2 November 2015.
Published online 16 December 2015.

1. Weaver, C. T., Hatton, R. D., Mangan, P. R. & Harrington, L. E. IL-17 family cytokines and the expanding diversity of effector T cell lineages. *Annu. Rev. Immunol.* **25,** 821–852 (2007).
2. Ivanov, I. I. *et al.* The orphan nuclear receptor RORγt directs the differentiation program of proinflammatory IL-17$^+$ T helper cells. *Cell* **126,** 1121–1133 (2006).
3. Leppkes, M. *et al.* RORγ-expressing Th17 cells induce murine chronic intestinal inflammation via redundant effects of IL-17A and IL-17F. *Gastroenterology* **136,** 257–267 (2009).
4. Genovese, M. C. *et al.* LY2439821, a humanized anti-interleukin-17 monoclonal antibody, in the treatment of patients with rheumatoid arthritis: a phase I randomized, double-blind, placebo-controlled, proof-of-concept study. *Arthritis Rheum.* **62,** 929–939 (2010).
5. Huh, J. R. *et al.* Digoxin and its derivatives suppress T_H17 cell differentiation by antagonizing RORγt activity. *Nature* **472,** 486–490 (2011).
6. Kondo, Y. *et al.* Involvement of RORγt-overexpressing T cells in the development of autoimmune arthritis in mice. *Arthritis Res. Ther.* **17,** 105 (2015).
7. Gaffen, S. L., Jain, R., Garg, A. V. & Cua, D. J. The IL-23–IL-17 immune axis: from mechanisms to therapeutic testing. *Nature Rev. Immunol.* **14,** 585–600 (2014).
8. Ciofani, M. *et al.* A validated regulatory network for Th17 cell specification. *Cell* **151,** 289–303 (2012).
9. O'Malley, B. W. & Kumar, R. Nuclear receptor coregulators in cancer biology. *Cancer Res.* **69,** 8217–8222 (2009).
10. Huang, Y. & Liu, Z. R. The ATPase, RNA unwinding, and RNA binding activities of recombinant p68 RNA helicase. *J. Biol. Chem.* **277,** 12810–12815 (2002).
11. Fuller-Pace, F. V. & Moore, H. C. RNA helicases p68 and p72: multifunctional proteins with important implications for cancer development. *Future Oncol.* **7,** 239–251 (2011).
12. Clark, E. L. *et al.* The RNA helicase p68 is a novel androgen receptor coactivator involved in splicing and is overexpressed in prostate cancer. *Cancer Res.* **68,** 7938–7946 (2008).
13. Linder, P. & Jankowsky, E. From unwinding to clamping — the DEAD box RNA helicase family. *Nature Rev. Mol. Cell Biol.* **12,** 505–516 (2011).
14. Arun, G., Akhade, V. S., Donakonda, S. & Rao, M. R. mrhl RNA, a long noncoding RNA, negatively regulates Wnt signaling through its protein partner Ddx5/p68 in mouse spermatogonial cells. *Mol. Cell. Biol.* **32,** 3140–3152 (2012).
15. Caretti, G. *et al.* The RNA helicases p68/p72 and the noncoding RNA SRA are coregulators of MyoD and skeletal muscle differentiation. *Dev. Cell* **11,** 547–560 (2006).
16. Lin, C., Yang, L., Yang, J. J., Huang, Y. & Liu, Z. R. ATPase/helicase activities of p68 RNA helicase are required for pre-mRNA splicing but not for assembly of the spliceosome. *Mol. Cell. Biol.* **25,** 7484–7493 (2005).
17. Jalal, C., Uhlmann-Schiffler, H. & Stahl, H. Redundant role of DEAD box proteins p68 (Ddx5) and p72/p82 (Ddx17) in ribosome biogenesis and cell proliferation. *Nucleic Acids Res.* **35,** 3590–3601 (2007).
18. Rosenbluh, J. *et al. RMRP* is a non-coding RNA essential for early murine development. *PLoS ONE* **6,** e26270 (2011).
19. Hsieh, C. L. *et al.* The gene for the RNA component of the mitochondrial RNA-processing endoribonuclease is located on human chromosome 9p and on mouse chromosome 4. *Genomics* **6,** 540–544 (1990).
20. Esakova, O. & Krasilnikov, A. S. Of proteins and RNA: the RNase P/MRP family. *RNA* **16,** 1725–1747 (2010).
21. Mäkitie, O., Kaitila, I. & Savilahti, E. Susceptibility to infections and *in vitro* immune functions in cartilage-hair hypoplasia. *Eur. J. Pediatr.* **157,** 816–820 (1998).
22. Bonafé, L. *et al.* Evolutionary comparison provides evidence for pathogenicity of *RMRP* mutations. *PLoS Genet.* **1,** e47 (2005).
23. Bacchetta, J. *et al.* Autoimmune hypoparathyroidism in a 12-year-old girl with McKusick cartilage hair hypoplasia. *Pediatr. Nephrol.* **24,** 2449–2453 (2009).
24. Jensen, E. D. *et al.* p68 (Ddx5) interacts with Runx2 and regulates osteoblast differentiation. *J. Cell. Biochem.* **103,** 1438–1451 (2008).
25. Dardenne, E. *et al.* RNA helicases DDX5 and DDX17 dynamically orchestrate transcription, miRNA, and splicing programs in cell differentiation. *Cell Rep.* **7,** 1900–1913 (2014).
26. Wortham, N. C. *et al.* The DEAD-box protein p72 regulates ERα-/oestrogen-dependent transcription and cell growth, and is associated with improved survival in ERα-positive breast cancer. *Oncogene* **28,** 4053–4064 (2009).
27. Ivanov, I. I. *et al.* Induction of intestinal Th17 cells by segmented filamentous bacteria. *Cell* **139,** 485–498 (2009).

28. Powrie, F. *et al.* Inhibition of Th1 responses prevents inflammatory bowel disease in scid mice reconstituted with CD45RB^{hi} CD4^{+} T cells. *Immunity* **1,** 553–562 (1994).
29. Hirota, K. *et al.* Fate mapping of IL-17-producing T cells in inflammatory responses. *Nature Immunol.* **12,** 255–263 (2011).
30. Wang, Y. *et al.* The transcription factors T-bet and Runx are required for the ontogeny of pathogenic interferon-γ-producing T helper 17 cells. *Immunity* **40,** 355–366 (2014).
31. Sun, Z. *et al.* Requirement for RORγ in thymocyte survival and lymphoid organ development. *Science* **288,** 2369–2373 (2000).
32. Chu, C., Quinn, J. & Chang, H. Y. Chromatin isolation by RNA purification (ChIRP). *J. Vis. Exp.* (2012).
33. Bonasio, R. & Shiekhattar, R. Regulation of transcription by long noncoding RNAs. *Annu. Rev. Genet.* **48,** 433–455 (2014).
34. Gomez, J. A. *et al.* The NeST long ncRNA controls microbial susceptibility and epigenetic activation of the interferon-γ locus. *Cell* **152,** 743–754 (2013).
35. Carpenter, S. *et al.* A long noncoding RNA mediates both activation and repression of immune response genes. *Science* **341,** 789–792 (2013).
36. Maenner, S., Muller, M., Frohlich, J., Langer, D. & Becker, P. B. ATP-dependent roX RNA remodeling by the helicase maleless enables specific association of MSL proteins. *Mol. Cell* **51,** 174–184 (2013).
37. Ilik, I. A. *et al.* Tandem stem-loops in roX RNAs act together to mediate X chromosome dosage compensation in *Drosophila*. *Mol. Cell* **51,** 156–173 (2013).
38. Calo, E. *et al.* RNA helicase DDX21 coordinates transcription and ribosomal RNA processing. *Nature* **518,** 249–253 (2015).
39. Yang, J., Sundrud, M. S., Skepner, J. & Yamagata, T. Targeting Th17 cells in autoimmune diseases. *Trends Pharmacol. Sci.* **35,** 493–500 (2014).
40. Lee, Y. J., Holzapfel, K. L., Zhu, J., Jameson, S. C. & Hogquist, K. A. Steady-state production of IL-4 modulates immunity in mouse strains and is determined by lineage diversity of iNKT cells. *Nature Immunol.* **14,** 1146–1154 (2013).
41. Takatori, H. *et al.* Lymphoid tissue inducer-like cells are an innate source of IL-17 and IL-22. *J. Exp. Med.* **206,** 35–41 (2009).
42. Luci, C. *et al.* Influence of the transcription factor RORγt on the development of NKp46^{+} cell populations in gut and skin. *Nature Immunol.* **10,** 75–82 (2009).
43. Chien, Y. H., Zeng, X. & Prinz, I. The natural and the inducible: interleukin (IL)-17-producing γδ T cells. *Trends Immunol.* **34,** 151–154 (2013).
44. Kang, H. S. *et al.* Gene expression profiling reveals a regulatory role for RORα and RORγ in phase I and phase II metabolism. *Physiol. Genomics* **31,** 281–294 (2007).
45. Yang, Y. *et al.* Focused specificity of intestinal T_H17 cells towards commensal bacterial antigens. *Nature* **510,** 152–156 (2014).
46. Sano, T. *et al.* An IL-23R/IL-22 circuit regulates epithelial serum amyloid A to promote local effector Th17 responses. *Cell* (2015).

Supplementary Information is available in the online version of the paper.

Acknowledgements We thank M. V. Pokrovskii for unpublished ATAC-seq data and L. X. Garmire for suggestions on our manuscript. This work was supported by a Cancer Research Institute Irvington Postdoctoral Fellowship (W.H.), Institutional NRSA T32 CA009161_Levy (W.H.), National Multiple Sclerosis Society postdoctoral fellowship FG 2089-A-1 (L.W.), Career Development Award (329388) from the Crohn's and Colitis Foundation of America (S.V.K.), Dale and Betty Frey Fellowship of the Damon Runyon Cancer Research Foundation 2105-12 (J.A.H.), HHMI Exceptional Research Opportunities Program (N.R.M. and N.H.), NIH F30 1F30CA189514-01 (R.A.F.), NIH P50-HG007735 and R01HG004361 (H.Y.C.), NIH R01AI080885 (D.R.L.), NIH R01DK103358 (R.B. and D.R.L.), and the Howard Hughes Medical Institute (H.Y.C. and D.R.L.).

Author Contributions W.H. and D.R.L. designed experiments, analysed data and wrote the manuscript with input from the co-authors; B.T. and O.A. performed mass spectrometry studies; F.Ri. designed and synthesized control and *Rmrp* ASOs; S.J.G. and L.W. performed MOG-EAE immunization and blinded scoring; S.V.K. performed blinded histology scoring on colitis sections; W.H. and A.I.D. designed and performed ribosome TRAP-seq studies. S.M. and R.M.M. performed library preparation for RNA sequencing studies; N.R.M. and N.G.H. performed microscopy studies; F.Ra. provided recombinant full length His-tagged hRORγt, and F.V.F.-P. generated DDX5 conditional mutant animals. J.A.H. performed RORγt ChIP studies. C.P.N performed DDX5 studies in the thymus. R.A.F., W.H. and H.Y.C. performed ChIRP-seq experiments. E.R.M and R.B. performed statistical analyses on ChIRP-seq experiments.

Author Information RNA-seq, TRAP-seq, RIP-seq, and ChIRP-seq data have been deposited in the Gene Expression Omnibus under accession number GSE70110. Reprints and permissions information is available at www.nature.com/reprints. The authors declare no competing financial interests. Readers are welcome to comment on the online version of the paper. Correspondence and requests for materials should be addressed to D.R.L. (dan.littman@med.nyu.edu).

METHODS

Data reporting. No statistical methods were used to predetermine sample size. The experiments were not randomized. In vivo transfer colitis and EAE mouse experiments were blinded, but cell culture and in vitro studies were not.

Mice. EEF1A1-LSL.EGFPL10 (lox-stop-lox-EGFP–L10 knockin at the *Ef1a1* locus) transgenic mice, RORγ/γt-deficient animals and *Ddx5*$^{fl/fl}$ mice have been previously described elsewhere[31,47,48]. Conditional mutant mice were bred to CD4-Cre transgenic animals (Taconic) and maintained on the C57BL/6 background. We bred heterozygous mice to yield 6–8-week-old *Ddx5*$^{+/+}$CD4-Cre^{+} (subsequently referred to as wild type) and *Ddx5*$^{fl/fl}$CD4-Cre^{+} (referred to as DDX5-T) littermates for experiments examining DDX5 in peripheral T-cell function. DDX5 conditional mutant mice were also bred to IL7R-Cre transgenic animals (Jackson Laboratory) (with *Ddx5* deleted in common early lymphoid progenitors; referred to as DDX5-clpKO) for experiments examining DDX5 functions during T-cell development in the thymus. *Rmrp*^{G270T} knock-in mice were generated using CRISPR-Cas9 technology by the Rodent Genetic Engineering Core (RGEC) at New York University Langone Medical Center. Guide RNA and homology directed repair donor template sequences are provided in Supplementary Table 1. Heterozygous crosses provided *Rmrp*$^{+/+}$ (wild-type) and *Rmrp*$^{G270T/G270T}$ littermates for *in vivo* studies. All animal procedures were in accordance with protocols approved by the Institutional Animal Care and Use Committee of the New York University School of Medicine (Animal Welfare Assurance number: A3435-01).

***In vivo* studies.** Steady-state small intestines were collected for isolation of lamina propria mononuclear cells as previously described[45]. For detecting SFB colonization, SFB-specific 16S primers were used[49]. Universal 16S and/or host genomic DNA was quantified simultaneously to normalize SFB colonization of each sample. All primer sequences are listed in Supplementary Table 1.

For the adoptive transfer model of colitis, 5×10^5 CD4^{+}CD25^{-}CD44^{low} CD45RB^{hi}CD62L^{hi} T cells were isolated from mouse splenocytes by FACS sorting and administered i.p. into *Rag2*$^{-/-}$ mice as previously described[50]. Animal weights were measured approximately weekly. Between weeks seven and eight, large intestines were collected for H&E staining and isolation of lamina propria mononuclear cells as previously described[45]. The H&E slides from each sample were examined in a double-blind fashion. The histology scoring (scale 0–24) was based on the evaluation of criteria described previously[51].

For induction of active EAE, each mouse was immunized subcutaneously on day 0 with 100 μg of MOG35–55 peptide, emulsified in CFA (Complete Freund's Adjuvant supplemented with additional 2 mg ml^{-1} *Mycobacterium tuberculosis*), and injected i.p. on days 0 and 2 with 100 ng per mouse of pertussis toxin (Calbiochem). The EAE scoring system was as follows: 0, no disease; 1, limp tail; 2, weak/partially paralysed hind legs; 3, completely paralysed hind legs; 4, complete hind and partial front leg paralysis; 5, complete paralysis/death.

In transfer colitis and EAE experiments, animals of different genotypes were co-housed and weighed and scored blindly. For statistical power level of 0.8, probability level of 0.05, anticipated effect size of 2, minimum sample size per group for two-tailed hypothesis is 6. Two-tailed unpaired Student's *t*-test was performed using Prism (GraphPad Software). We treated a *P* value of less than 0.05 as a significant difference. All experiments were performed at least twice.

***In vitro* T-cell culture and phenotypic analysis.** Mouse T cells were purified from lymph nodes and spleens of 6–8-week-old mice, by sorting live (DAPI^{-}), CD8^{-}CD19^{-}CD4^{+}CD25^{-}CD44$^{low/int}$CD62L^{+} naive T cells using a FACSAria (BD). Detailed antibody information is provided in Supplementary Table 1. Cells were cultured in Iscove's Modified Dulbecco's Medium (IMDM, Sigma) supplemented with 10% heat-inactivated FBS (Hyclone), 50 U penicillin-streptomycin (Invitrogen), 4 mM glutamine and 50 μM β-mercaptoethanol. For T-cell polarization, 200 μl of cells was seeded at 0.3×10^5 cells per ml in 96-well plates precoated with goat anti-hamster IgG at a 1:20 dilution of stock (1 mg ml^{-1}, MP Biomedicals). Naive T cells were activated with anti-CD3 ε (2.5 μg ml^{-1}) and anti-CD28 (10 μg ml^{-1}). Cells were cultured for 4–5 days under T$_H$17-polarizing conditions (0.1–0.3 ng ml^{-1} TGF-β, 20 ng ml^{-1} IL-6), T$_H$1- (10 ng ml^{-1} IL-12, 10 U ml^{-1} IL-2), T$_H$2- (10 ng ml^{-1} IL-4, 10 U ml^{-1} IL-2), or T$_{reg}$- (5 ng ml^{-1} TGF-β, 10 U ml^{-1} IL-2) conditions.

Human T cells were isolated from peripheral blood of healthy donors using anti-human CD4 MACS beads (Miltenyi). Human CD4^{+} T cells were cultured in 96-well U bottom plates in 10 U ml^{-1} of IL-2, 10 ng ml^{-1} of IL-1β, 10 ng ml^{-1} of IL-23, 1 μg ml^{-1} of anti-IL-4, 1 μg ml^{-1} of anti-IFNγ and anti-CD3/CD28 activation beads (LifeTechnologies) at a ratio of 1 bead per cell, as previously described[52].

For cytokine analysis, cells were incubated for 5 h with phorbol 12-myristate 13-acetate (PMA) (50 ng ml^{-1}; Sigma), ionomycin (500 ng ml^{-1}; Sigma) and GolgiStop (BD). Intracellular cytokine staining was performed according to the manufacturer's protocol (Cytofix/Cytoperm buffer set from BD Biosciences and FoxP3 staining buffer set from eBioscience). A LSR II flow cytometer (BD Biosciences) and FlowJo (Tree Star) software were used for flow cytometry and analysis. Dead cells were excluded using the Live/Dead fixable aqua dead cell stain kit (Invitrogen).

Nucleic acid reagents and T-cell transduction. Custom *Rmrp* and predesigned *Malat1* Stellaris RNA fluorescence *in situ* hybridization (FISH) probes were purchased from BiosearchTech and used to label mouse *Rmrp* and *Malat1* RNA in cultured T$_H$17 cells according to the manufacturer's protocol. Control and human *DDX5*-specific short interfering RNAs (siRNAs) were obtained from Cell Signaling. Synthesis of ASOs was performed as previously described[53]. All ASOs were 20 nucleotides in length and had a phosphorothioate backbone. The ASOs had five nucleotides at the 5′ and 3′ ends modified with 2′-*O*-methoxyethyl (MOE) for increased stability. ASOs and siRNA sequences are provided in Supplementary Table 1. siRNA and ASOs were introduced into mouse T$_H$17 cells by Amaxa nucleofection as previously described[8].

Wild-type and helicase-dead mutant DDX5 were described previously[54]. DDX5 and *Rmrp* were subcloned into the mouse stem-cell virus (MSCV) Thy1.1 vectors for retroviral overexpression and rescue assays in T cells. Retrovirus production was carried out in Plat-E cells (Cell Biolabs, Inc., not tested for mycoplasma) as previously described[55]. Spin transduction was performed 24 h after *in vitro* T-cell activation by centrifugation in a Sorvall Legend RT at 700 *g* for 90 min at 32 °C. Aqua^{-}Thy1.1^{+} live and transduced cells were analysed by flow cytometry after 5 days of culture in T$_H$17-polarizing conditions.

RORγt transcriptional activity in polarized T$_H$17 cells. A ROR luciferase reporter was constructed with four RORE sites replacing the Gal4 (UAS) sites from the pGL4.31 vector (luc2P/GAL4 UAS/Hygro) from Promega (C935A) as described in ref. 56. Naive CD4^{+} T cells were cultured in T$_H$17-polarizing conditions for 72 h. Nucleofection (Amaxa Nucleofector 4D, Lonza) was then used to introduce 1 μg RORE–firefly luciferase reporter construct and 1 μg control *Renilla* luciferase construct according to the manufacturer's instructions. Luciferase activity was measured using the dual luciferase reporter kit (Promega) at 24 h after transfection. Relative luciferase units (RLU) were calculated as a function of firefly luciferase reads over those of *Renilla* luciferase. DMSO or 2 μM RORγ inhibitor (ML209) were used in luciferase experiments as described in ref. 57.

Co-immunoprecipitation and mass spectrometry. Cultured T$_H$17 cells (100×10^6) were lysed in 25 mM Tris (pH 8.0), 100 mM NaCl, 0.5% NP-40, 10 mM $MgCl_2$, 10% glycerol, 1× protease inhibitor and PhosphoSTOP (Roche) on ice for 30 min, followed by homogenization with a 25-gauge needle. The RORγ/γt-specific antibody used for pull-down assays was previously described[8]. Co-immunoprecipitated complexes were collected with protein G dynabeads (Dynal, Invitrogen). Detailed antibody information is provided in Supplementary Table 1. Mass spectrometry and the Mascot database search to identify protein complex composition were both performed by the Central Proteomics Facility at the Dunn School of Pathology, Oxford, UK.

Ribosome TRAP-seq, RIP-seq and RNA-seq. Twenty million cells cultured in T$_H$17-polarizing conditions for 48 h were lysed in 10 mM HEPES (pH 7.4), 150 mM KCl, 5 mM $MgCl_2$, 0.5 mM dithiothreitol (DTT), 100 μg ml^{-1} cycloheximide, 1% NP-40, 30 mM DHPC, 1× protease inhibitor and PhosphoSTOP (Roche). Ribosome-TRAP immunoprecipitation was first performed using 2 μg of anti-GFP antibody (Invitrogen) and collected in 20 μl of protein G magnetic dynabeads. The supernatant was removed for subsequent RIP pull-down using anti-DDX5 (Abcam) or anti-RORγt antibodies and collected with protein G dynabeads. TRAP-seq samples were washed with high-salt wash buffer (10 mM HEPES (pH 7.4), 350 mM KCl, 5 mM $MgCl_2$, 1% NP-40, 0.5 mM DTT and 100 μg ml^{-1} cycloheximide). RIP-seq samples were washed three times with 25 mM Tris (pH 8.0), 100 mM NaCl, 0.5% NP-40, 10 mM $MgCl_2$, 10% glycerol, 1× protease inhibitor and PhosphoSTOP (Roche). Enrichment of target proteins was confirmed by immunoblot analysis. Complementary DNAs (cDNAs) were synthesized from TRIzol (Invitrogen)-isolated RNA, using Superscript III kits (Invitrogen). RNA-seq libraries were prepared and sequenced at Genome Services Laboratory, HudsonAlpha. Sequencing reads were mapped by Tophat and transcripts called by Cufflinks. Pull-down enrichment was calculated for each transcript as a ratio of FPKM recovered from TRAP-seq and RIP-seq samples compared to those from 5% input.

For RNA-seq analysis, volcano scores for wild-type, DDX5-T and RORγt-knockout T$_H$17 cells were calculated for each transcript as a function of its *P* value and fold change between mutant and wild-type controls. BAM files were converted to .tdf format for viewing with the IGV Browser Tool. Ingenuity Pathway Analysis (IPA, Qiagen) was used to identify enriched Gene Ontology terms in the DDX5–RORγt coregulated gene set.

ChIRP-seq and ChIRP-qPCR. The ChIRP-seq assay was performed largely as described previously[58]. Mouse T$_H$17 cells were cultured as above and *in vivo* RNA–chromatin interactions were fixed with 1% glutaraldehyde for 10 min at 25 °C. Antisense DNA probes (designated 'odd' or 'even') against *Rmrp* were designed

by Biosearch Probe Designer (1, 5′-TAGGAAACAGGCCTTCAGAG-3′; 2, 5′-AACATGTCCCTCGTATGTAG-3′; 3, 5′-CCCCTAGGCGAAAGGATAAG-3′; 4, 5′-AACAGTGACTTGCGGGGGAA-3′; 5, 5′-CTATGTGAGCTGACGG ATGA-3′). Probes modified with BiotinTEG at the 3′ end were synthesized by Integrated DNA Technologies (IDT). Isolated RNA was used in RT–qPCR analysis (Stratagene) to quantify enrichment of *Rmrp* and depletion of other cellular RNAs. Isolated DNA was used for qPCR analysis or to make deep sequencing libraries with the NEBNext DNA library prep master mix set for Illumina (NEB). Library DNA was quantified on the high sensitivity bioanalyzer (Agilent) and sequenced from a single end for 75 cycles on an Illumina NetSeq 500.

Sequencing reads were first trimmed of adaptors (FASTX Toolkit) and then mapped using Bowtie to a custom bowtie index containing single-copy loci of repetitive RNA elements (ribosomal RNAs, small nuclear RNAs, and noncoding Y RNAs[59]). Reads that did not map to the custom index were then mapped to mm9. Mapped reads were separately shifted towards the 3′ end using MACS and normalized to a total of 10 million reads. Even and odd replicates were merged as described previously[58] by taking the lower of the two read density values at each nucleotide across the entire genome. These processing steps take raw FASTQ files and yield processed files that contain genome-wide *Rmrp*-occupied chromatin association maps, where each nucleotide in the genome has a value that represents the relative binding level of the *Rmrp* RNA. MACS parameters were as follows: band width = 300; model fold = 10, 30; *P*-value cutoff = 1×10^5. The full pipeline is available at https://github.com/bdo311/chirpseq-analysis.

ChIRP-qPCR was performed on DNA purified after treatment with RNase (60 min, 37 °C) and proteinase K (45 min, 65 °C). The primers used for qPCR are listed in Supplementary Table 1. For enrichment analysis, we tested for the enrichment of *Rmrp* ChIRP peaks among ChIP peak sets for key T_H17 transcription factors, CTCF, RNA Pol II and several histone marks[8]. Assay for transposase-accessible chromatin sequencing (ATAC)-seq was performed, according to published protocol[60], on cultured T_H17-polarized cells *in vitro* for 48 h (unpublished data). Because of differences in ChIP antibody affinities and the bias in the selection of ChIP and ChIRP factors, we used peaks generated from ATAC-seq data as a background setting for the enrichment analysis. In our analysis, we considered all ChIRP and ChIP peaks that fell within ±500 base pairs of ATAC-seq peaks, and then calculated the overlap among the ChIRP and ChIP sets, using the hypergeometric distribution to estimate significance.

***In vitro* binding assay.** For *in vitro* binding assays, pcDNA3.1-Rmrp vectors were used for T7 polymerase-driven *in vitro* transcription (IVT) reactions (Promega). Haemagglutinin (HA)–DDX5 and Flag–RORγt were *in vitro* transcribed and translated using an *in vitro* transcription and translation (TNT) system according to the manufacturer's protocol (Promega). Alternatively, pGEX4.1-DDX5 (wild-type and helicase-dead mutant) constructs were transformed into BL21 to synthesize recombinant full-length GST–hDDX5 proteins. Full-length His-tagged human RORγt was purified in three steps through Ni-resin, S column and gel-filtration (AKTA). Then, 0.5 μg of each recombinant protein was incubated in the presence or absence of 200 μM ATP, 300 ng *in vitro* transcribed *Rmrp* in co-immunoprecipitation buffer containing 25 mM Tris (pH 8.0), 100 mM NaCl, 0.5% NP-40, 10 mM $MgCl_2$, 10% glycerol, 1× protease inhibitor, RNaseInhibitor (Invitrogen) and PhosphoSTOP (Roche). GST–DDX5 was enriched on glutathione beads (GE); HA–DDX5, Flag–RORγt and His–RORγt were enriched using anti-HA (Covance), anti-Flag (Sigma) and anti-His antibodies (Santa Cruz Bio) coupled to anti-mouse immunoglobulin dynabeads (Dynal, Invitrogen).

Microscopy. T_H17 cells were cultured on glass coverslips for 48 h and fixed in 4% paraformaldehyde in PBS for 5 min at room temperature. Fixed cells were permeabilized with 0.1% bovine serum albumin (BSA), 0.1% Triton and 10% normal serum in PBS for 1 h. Cells were then incubated with primary antibodies (DDX5 (Abcam) or RORγt (eBiosciences)) in 0.1% BSA and 0.2% Triton PBS overnight at 4 °C. Secondary antibodies (anti-goat Alexa 488 or anti-rat Alexa 647 (Molecular Probe)) were incubated at 4 °C for 1 h. Stained cells were washed three times with 0.5% Tween and 0.1% BSA in PBS. DAPI was used to stain DNA inside the nucleus. Immunofluorescence images were captured on a Zeiss 510 microscope at 40×.

ChIP and RT–qPCR analysis. T_H17-polarized cells were crosslinked with 1% paraformaldehyde (EMS) and incubated with rotation at room temperature. Crosslinking was stopped after 10 min with glycine to a final concentration of 0.125 M and incubated for a further 5 min with rotation. Cells were washed with 3× ice-cold PBS and pellets were either flash-frozen in liquid N_2 or immediately resuspended in Farnham lysis buffer (5 mM PIPES, 85 mM KCl, 0.5% NP-40). Hypotonic lysis continued for 10 min on ice before cells were spun down and resuspended in RIPA buffer (1× PBS, 1% NP-40, 0.5% SDS, 0.5% Na-deoxycholate), transferred into TPX microtubes and lysed on ice for 30 min. Nuclear lysates were sonicated for 40 cycles of 30 s 'ON' and 30 s 'OFF' in 10-cycle increments using a Biorupter (Diadenode) set on high. After pelleting debris, chromatin was precleared with protein G dynabeads (dynabeads, TFS) for 2 h with rotation at 4 °C. For immunoprecipitation, precleared chromatin was incubated with anti-RORγt antibodies (1 μg per 2×10^6 cells) overnight with rotation at 4 °C and protein G was added for the final 2 h of incubation. Beads were washed and bound chromatin was eluted. ChIP-qPCR was performed on DNA purified after treatment with RNase (30 min, 37 °C) and proteinase K (2 h, 55 °C) followed by reversal of crosslinks (8–12 h, 65 °C). The primers used for qPCR have been described previously[5].

For analysis of mRNA transcripts, gene specific values were normalized to the *Gapdh* housekeeping gene for each sample. All primer sequences are listed in Supplementary Table 1.

47. Stanley, S. *et al.* Profiling of glucose-sensing neurons reveals that GHRH neurons are activated by hypoglycemia. *Cell Metab.* **18,** 596–607 (2013).
48. Nicol, S. M. *et al.* The RNA helicase p68 (DDX5) is selectively required for the induction of p53-dependent p21 expression and cell-cycle arrest after DNA damage. *Oncogene* **32,** 3461–3469 (2013).
49. Croswell, A., Amir, E., Teggatz, P., Barman, M. & Salzman, N. H. Prolonged impact of antibiotics on intestinal microbial ecology and susceptibility to enteric *Salmonella* infection. *Infect. Immun.* **77,** 2741–2753 (2009).
50. Ostanin, D. V. *et al.* T cell transfer model of chronic colitis: concepts, considerations, and tricks of the trade. *Am. J. Physiol. Gastrointest. Liver Physiol.* **296,** G135–G146 (2009).
51. Kim, S. V. *et al.* GPR15-mediated homing controls immune homeostasis in the large intestine mucosa. *Science* **340,** 1456–1459 (2013).
52. Manel, N., Unutmaz, D. & Littman, D. R. The differentiation of human T_H-17 cells requires transforming growth factor-β and induction of the nuclear receptor RORgammat. *Nature Immunol.* **9,** 641–649 (2008).
53. Meng, L. *et al.* Towards a therapy for Angelman syndrome by targeting a long non-coding RNA. *Nature* **518,** 409–412 (2015).
54. Bates, G. J. *et al.* The DEAD box protein p68: a novel transcriptional coactivator of the p53 tumour suppressor. *EMBO J.* **24,** 543–553 (2005).
55. Morita, S., Kojima, T. & Kitamura, T. Plat-E: an efficient and stable system for transient packaging of retroviruses. *Gene Ther.* **7,** 1063–1066 (2000).
56. Santori, F. R. *et al.* Identification of natural RORγ ligands that regulate the development of lymphoid cells. *Cell Metab.* **21,** 286–297 (2015).
57. Huh, J. R. *et al.* Identification of potent and selective diphenylpropanamide RORgamma Inhibitors. *ACS Med. Chem. Lett.* **4,** 79–84, (2013).
58. Chu, C., Qu, K., Zhong, F. L., Artandi, S. E. & Chang, H. Y. Genomic maps of long noncoding RNA occupancy reveal principles of RNA-chromatin interactions. *Mol. Cell* **44,** 667–678 (2011).
59. Flynn, R. A. *et al.* Dissecting noncoding and pathogen RNA–protein interactomes. *RNA* **21,** 135–143 (2015).
60. Buenrostro, J. D., Wu, B., Chang, H. Y. & Greenleaf, W. J. ATAC-seq: a method for assaying chromatin accessibility genome-wide. *Curr. Protoc. Mol. Biol.* **109,** 21.29.1–21.29.9. (2015).

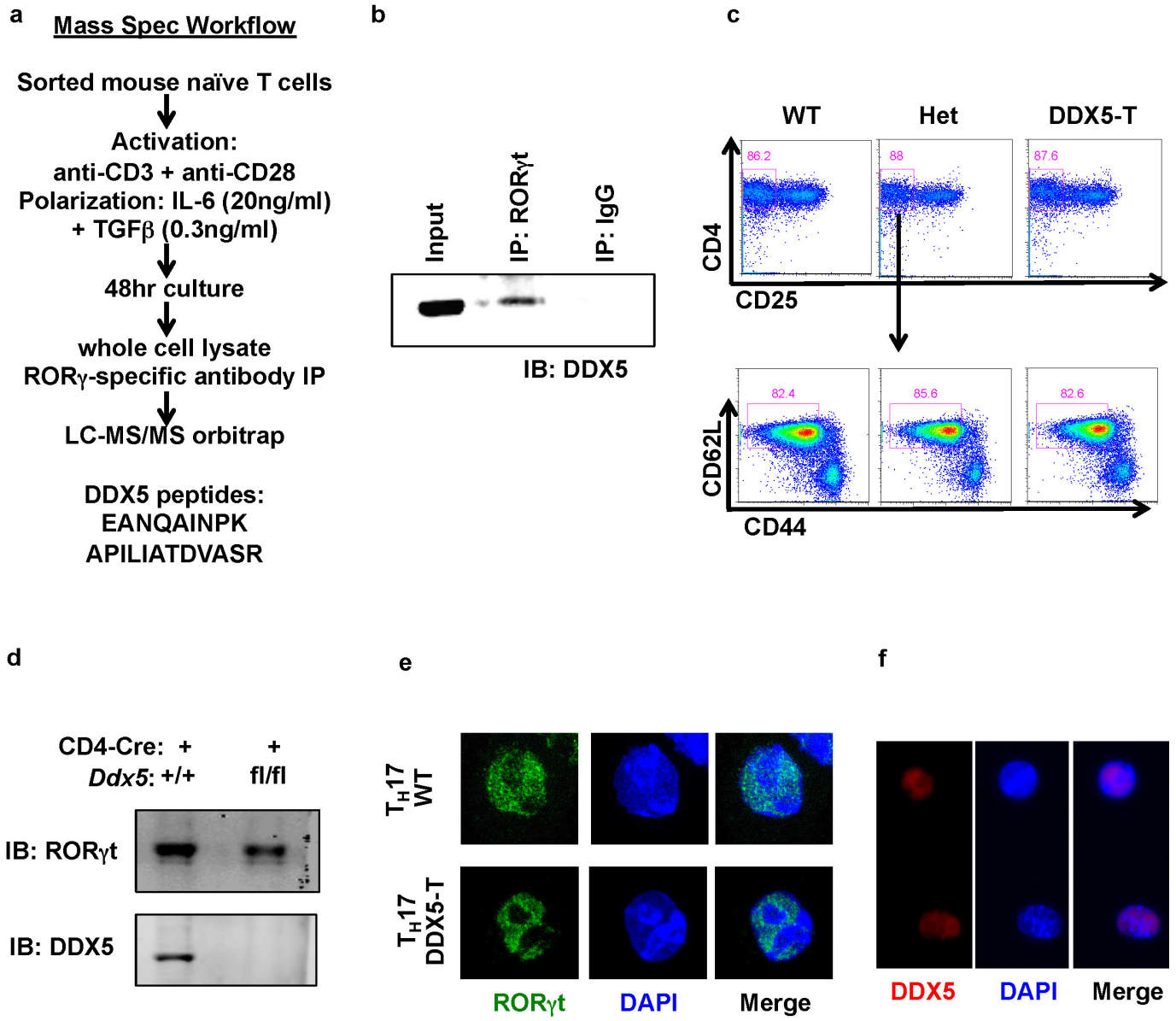

Extended Data Figure 1 | Identification of DDX5 as a RORγt-interacting partner. a, Mass spectrometry experimental workflow. Sorted naive $CD4^+$ T cells from wild-type mice were cultured *in vitro* in T_H17-polarizing conditions for 48 h. Immunoprecipitation of endogenous RORγt was performed using RORγ/γt-specific antibodies on whole-cell lysates. RORγt enrichment in pull-down was confirmed by immunoblot. Immunoprecipitated proteins were digested and analysed by mass spectrometry. The listed DDX5 peptides were identified in the T_H17 RORγt immunoprecipitate. **b**, Co-immunoprecipitaton of DDX5 with anti-RORγt in lysates of *in vitro* polarized T_H17 cells. **c**, Cell surface phenotype of splenic and lymph node $DAPI^-CD4^+CD8\alpha^-CD19^-$ T cells from wild-type and DDX5-T mice, examined by flow cytometry. **d**, Immunoblot of RORγt protein expression whole-cell lysate of cultured T_H17 cells from wild-type or DDX5-T animals. For uncropped gels (**b**, **d**), see Supplementary Fig. 1. **e**, Immunofluorescence staining of RORγt in cultured T_H17 cells from wild-type or DDX5-T mice. **f**, Immunofluorescence staining revealed nuclear localization of DDX5 in T_H17 cells.

a

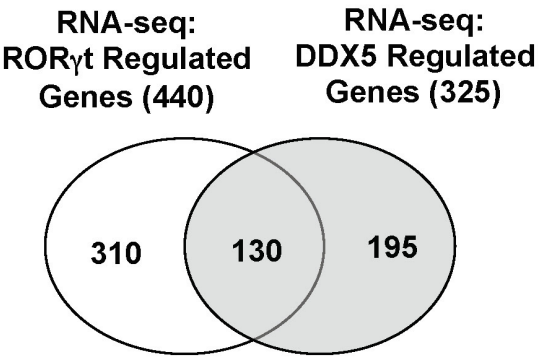

b

DDX5-RORγt coregulated genes	
Ingenuity Canonical Pathways	-log (p-value)
T Helper Cell Differentiation	5.33
Communication between Innate and Adaptive Immune Cells	2.65
Interleukin Signaling and Production	2.08

c

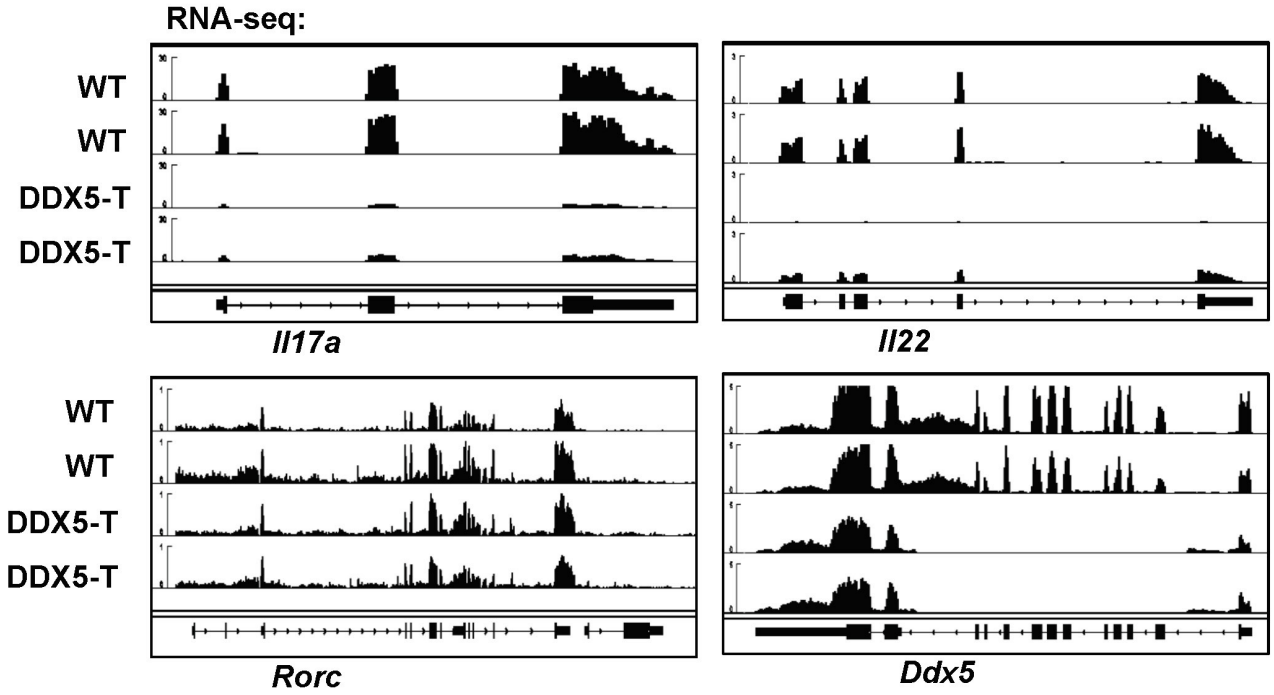

d

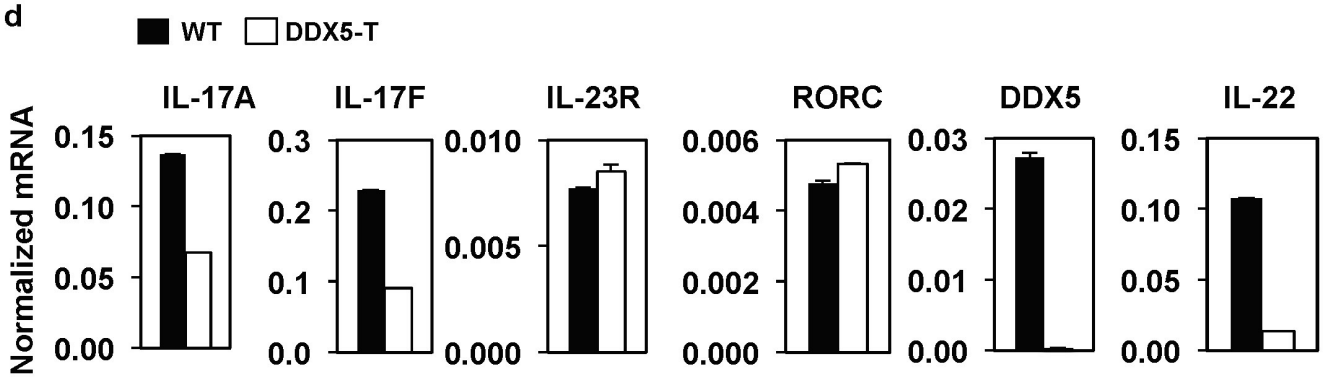

Extended Data Figure 2 | DDX5 coregulates a subset of RORγt transcriptional targets in polarized T_H17 cells. a, Venn diagram of distinct and overlapping genes regulated by RORγt and/or DDX5, as determined from RNA-seq studies. **b**, Ingenuity Pathway Analysis (Qiagen) of DDX5- and RORγt-coregulated genes. **c**, IGV browser view showing biological replicate RNA-seq coverage tracks of control and DDX5-T from *in vitro* polarized T_H17 cell samples at the *Il17a*, *Il22*, *Ddx5* and *Rorc* loci. **d**, Independent RT–qPCR validation of RNA-seq results confirming effects of DDX5 deletion on RORγt target gene expression. Graphs show mean ± s.d.

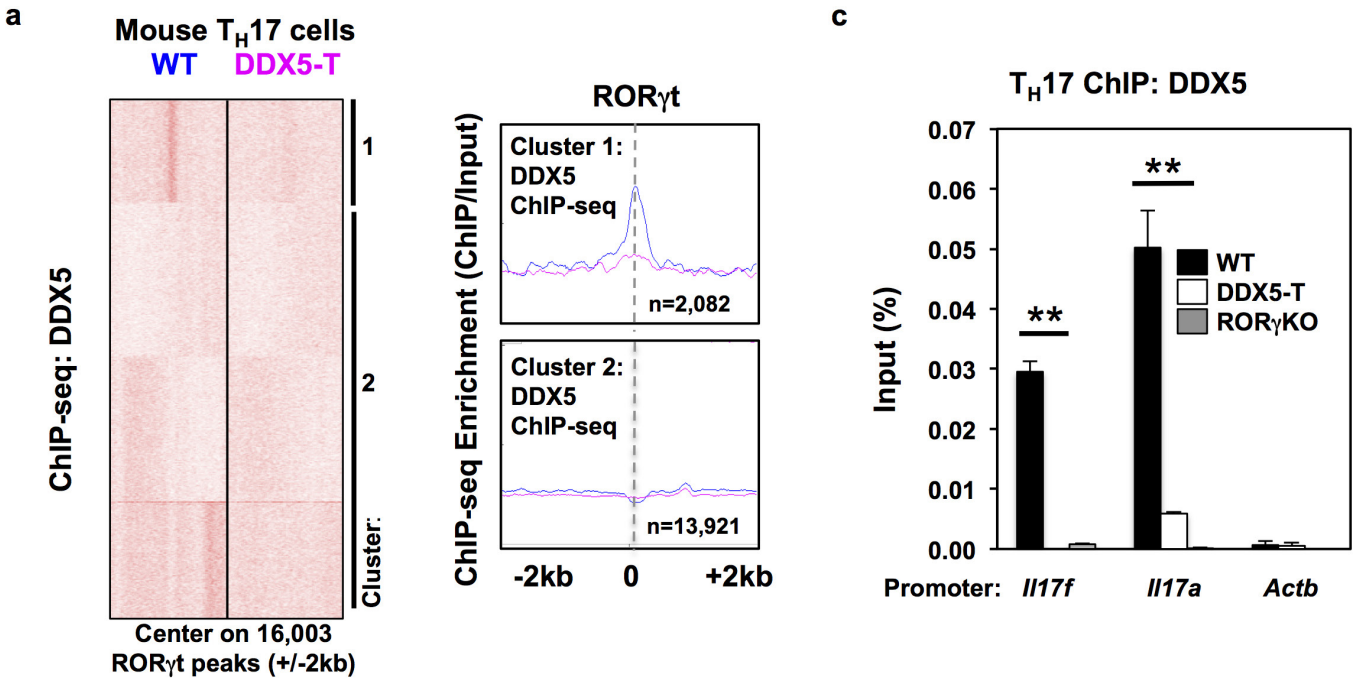

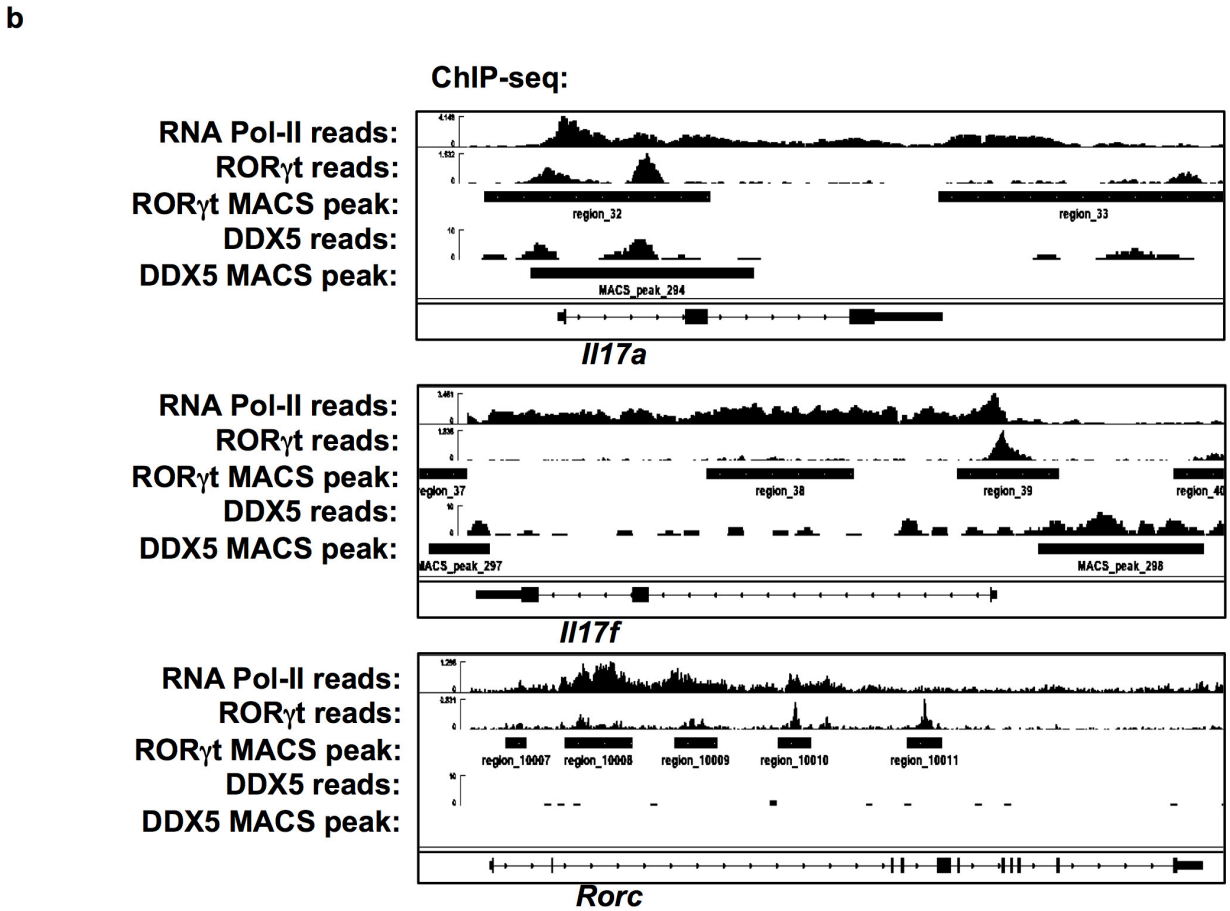

Extended Data Figure 3 | DDX5 chromatin localization in T$_H$17 cells. **a**, ChIP-seq-generated heatmap of DDX5 occupancy in regions centred on 16,003 RORγt-occupied sites (±2 kilobases (kb)). *K*-means linear normalization was used for clustering analysis by SeqMiner. Metagene analysis on cluster 1 depicts RORγt-occupied regions with DDX5 enrichment in wild-type but not DDX5-T cells; cluster 2 represents RORγt-occupied regions without DDX5 enrichment. **b**, IGV browser view of *Il17a*, *Il17f* and *Rorc* loci with ChIP-seq enrichment for RNA Pol II, RORγt and DDX5. **c**, Independent ChIP-qPCR of DDX5 in polarized T$_H$17 cells. DDX5 occupancy at the *Il17a* and *Il17f* loci (as identified by RORγt ChIP-seq MACS peak called 32 and 39, respectively, from **b**) in control, DDX5-T or RORγt-deficient (RORγKO) cells. Results are representative of two independent experiments. Each experiment was performed with two technical replicates. Graph shows mean ± s.d. $^{**}P < 0.01$ (unpaired, *t*-test).

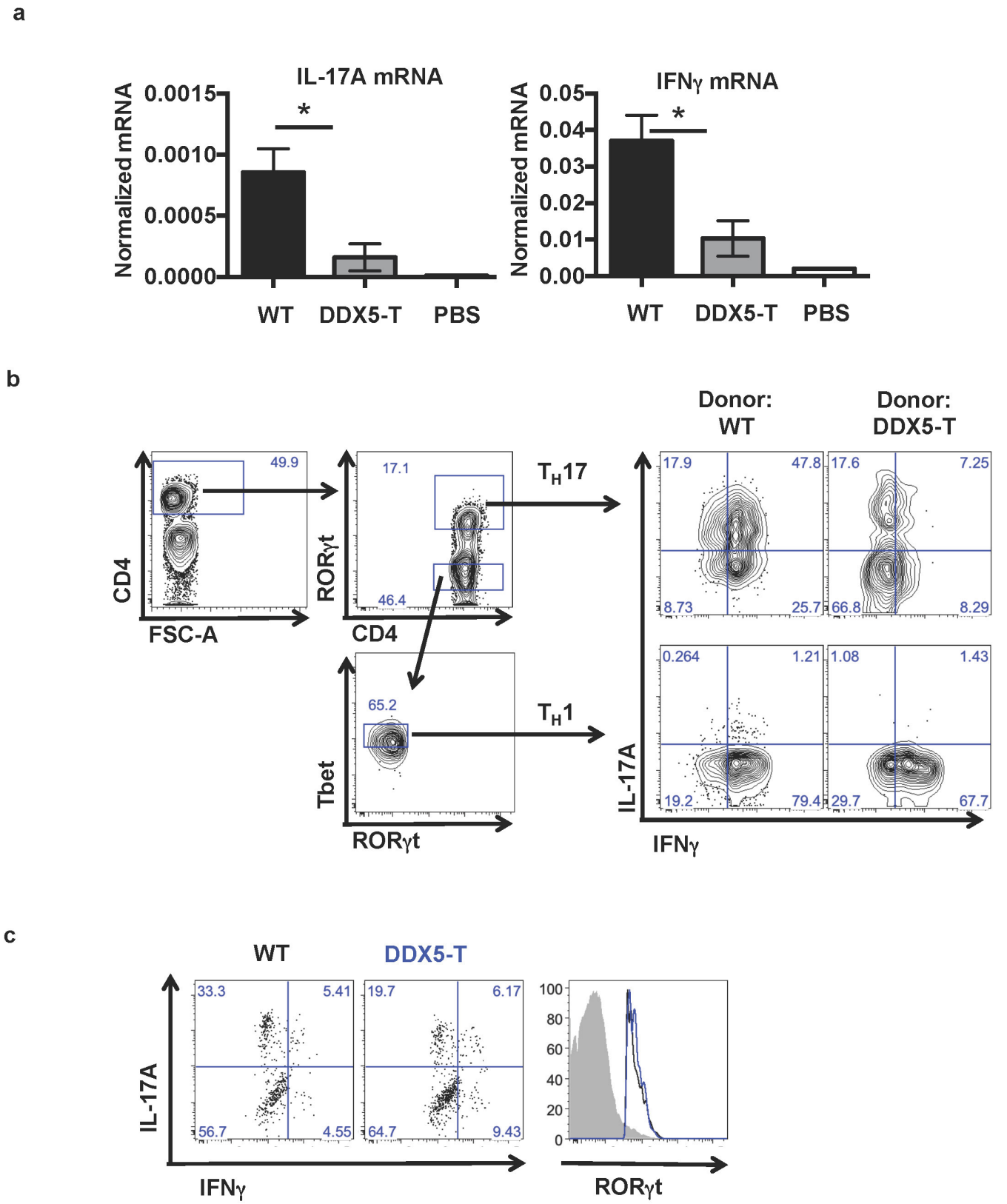

Extended Data Figure 4 | Influence of DDX5 on T-cell phenotypes in autoimmune disease models. a, At 8 weeks after T-cell transfer, large intestine lamina propria mononuclear cells were evaluated for amounts of *Il17a* and *Ifng* mRNA by RT–qPCR. Results are representative of two independent experiments. Each experiment was performed using large intestines from three mice in each condition. RT–qPCR was performed with two technical replicates. Graph shows mean ± s.d. $*P < 0.03$ (unpaired, *t*-test). **b**, Gating strategy for analysis of T_H17 and T_H1 cells from large intestine of Rag2-deficient recipients of wild-type or DDX5-T naive T cells analysed at 8 weeks after T-cell transfer. **c**, Representative IL-17A and IFNγ intracellular staining of Aqua$^-$CD4$^+$RORγt$^+$ T_H17 cells in spinal cord of MOG-immunized animals on day 21.

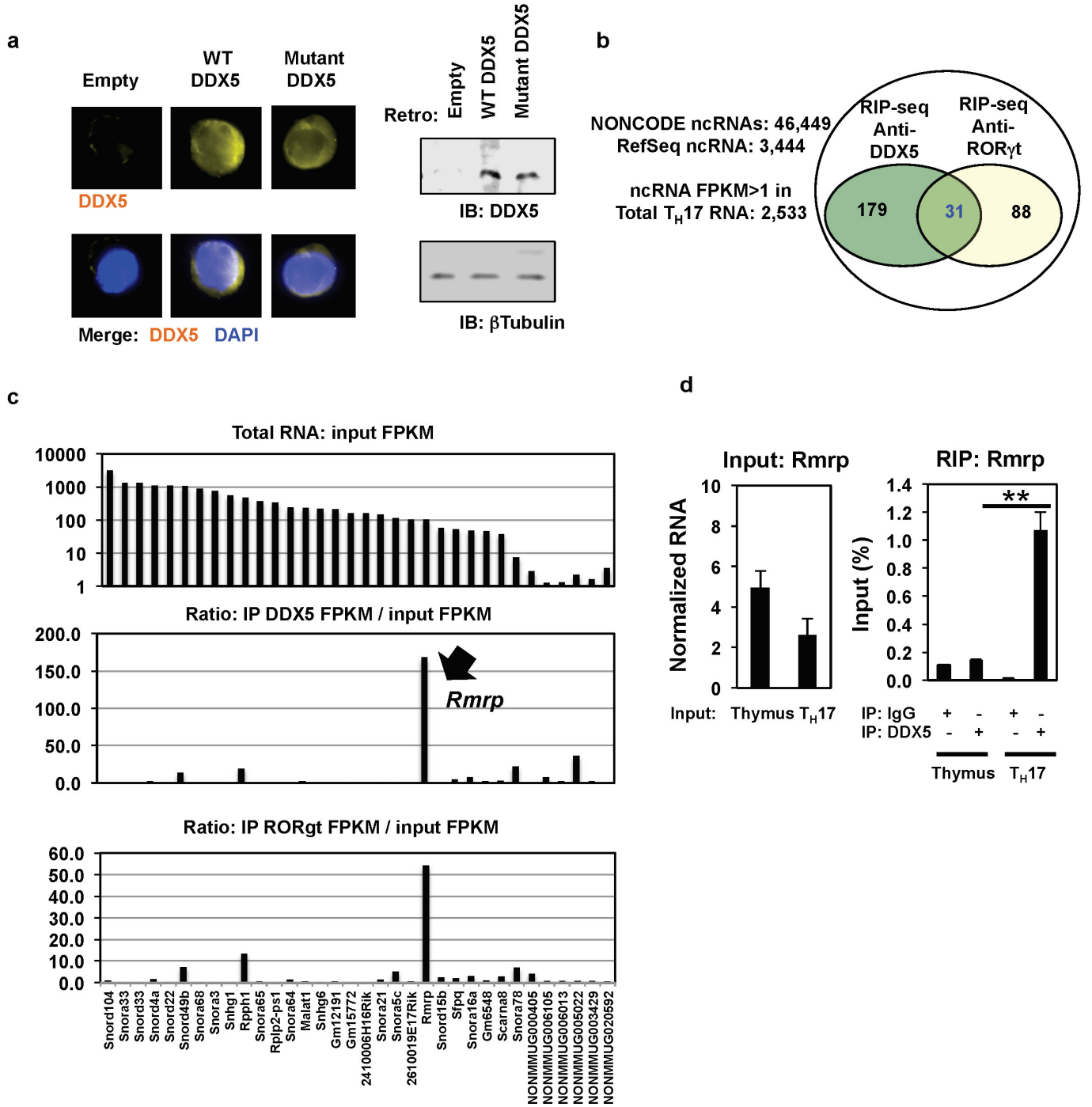

Extended Data Figure 5 | Noncoding RNAs enriched in DDX5 and RORγt RIP-seq studies. a, DDX5-T cells were transduced with wild-type or helicase-mutant DDX5 and evaluated for DDX5 expression by immunofluorescence (left) and immunoblot (right) with anti-DDX5 antibody. For uncropped gels, see Supplementary Fig. 1. **b**, Venn diagram of noncoding RNAs detected by RIP-seq of ribosome-depleted T_H17 cell lysates with anti-DDX5 and anti-RORγt antibodies. **c**, Abundance of top noncoding RNAs enriched in DDX5 and RORγt immunoprecipitates from polarized T_H17 cell lysates depleted of ribosomes. Top, abundance of the noncoding RNAs in total lysate. **d**, RIP-qPCR experiments to compare *Rmrp* association with DDX5 in cultured T_H17 and total thymocytes *ex vivo*. Results are representative of three independent experiments. Each experiment was performed with two technical replicates. Graph shows mean ± s.d. $^{**}P < 0.001$ (unpaired, *t*-test).

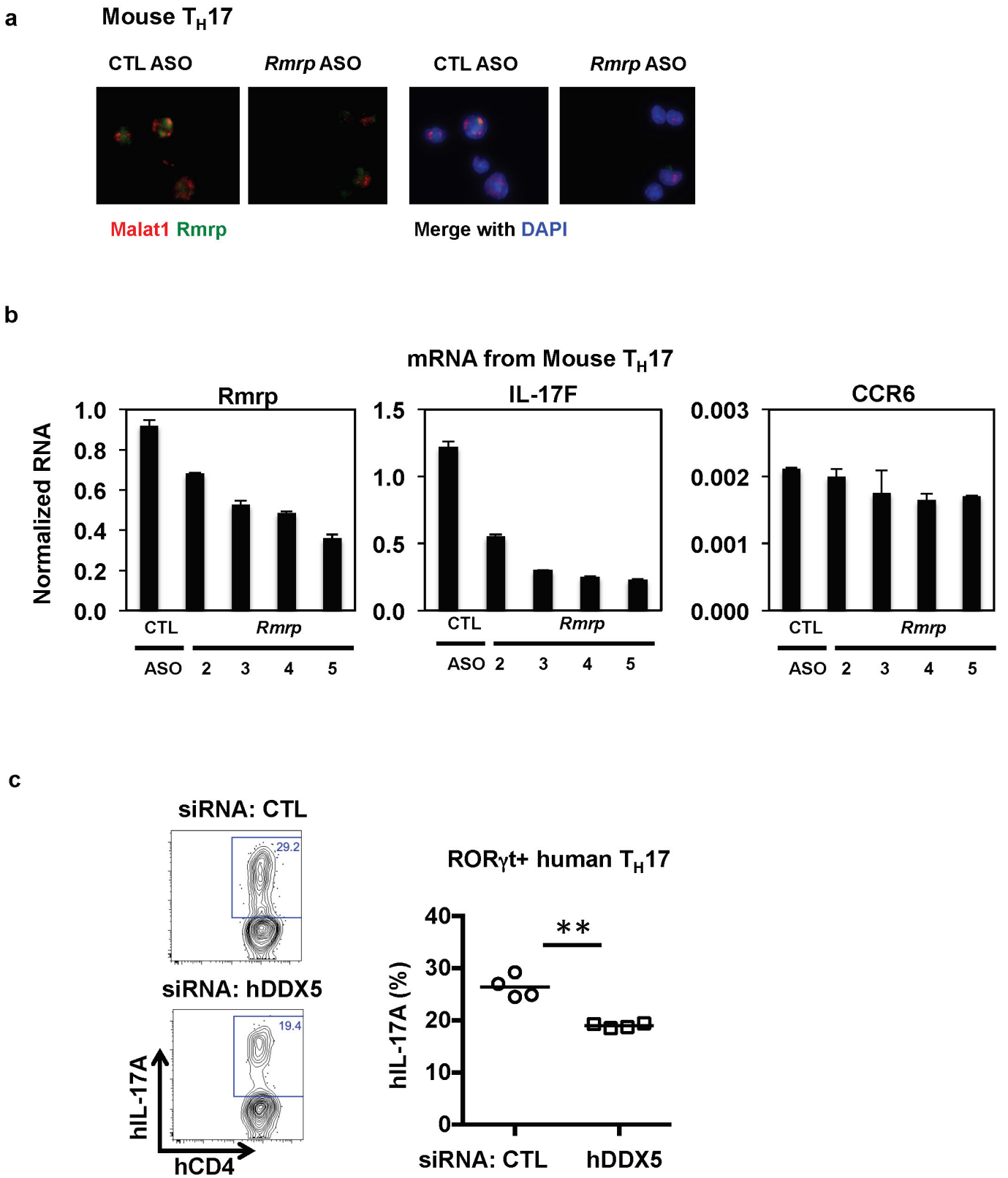

Extended Data Figure 6 | *Rmrp* and DDX5 knockdown in mouse and human T_H17 cells. a, RNA FISH analysis, using probes specific for *Rmrp* (green) and *Malat1* (red) lncRNAs, in T_H17 cells at 72 h after nucleofection with control (CTL) or *Rmrp* ASOs. **b**, Effect of *Rmrp* ASOs targeting different regions of *Rmrp* transcript on levels of *Rmrp*, *Il17f* and *Ccr6* RNAs in polarized T_H17 cells. **c**, Knockdown of DDX5 reduced IL-17A production in *in vitro* polarized human RORγt^+ T_H17 cells. $^{**}P < 0.01$ (paired, *t*-test). Representative result shown in left panel. Each dot represents a different healthy donor ($n = 4$). Graphs show mean ± s.d.

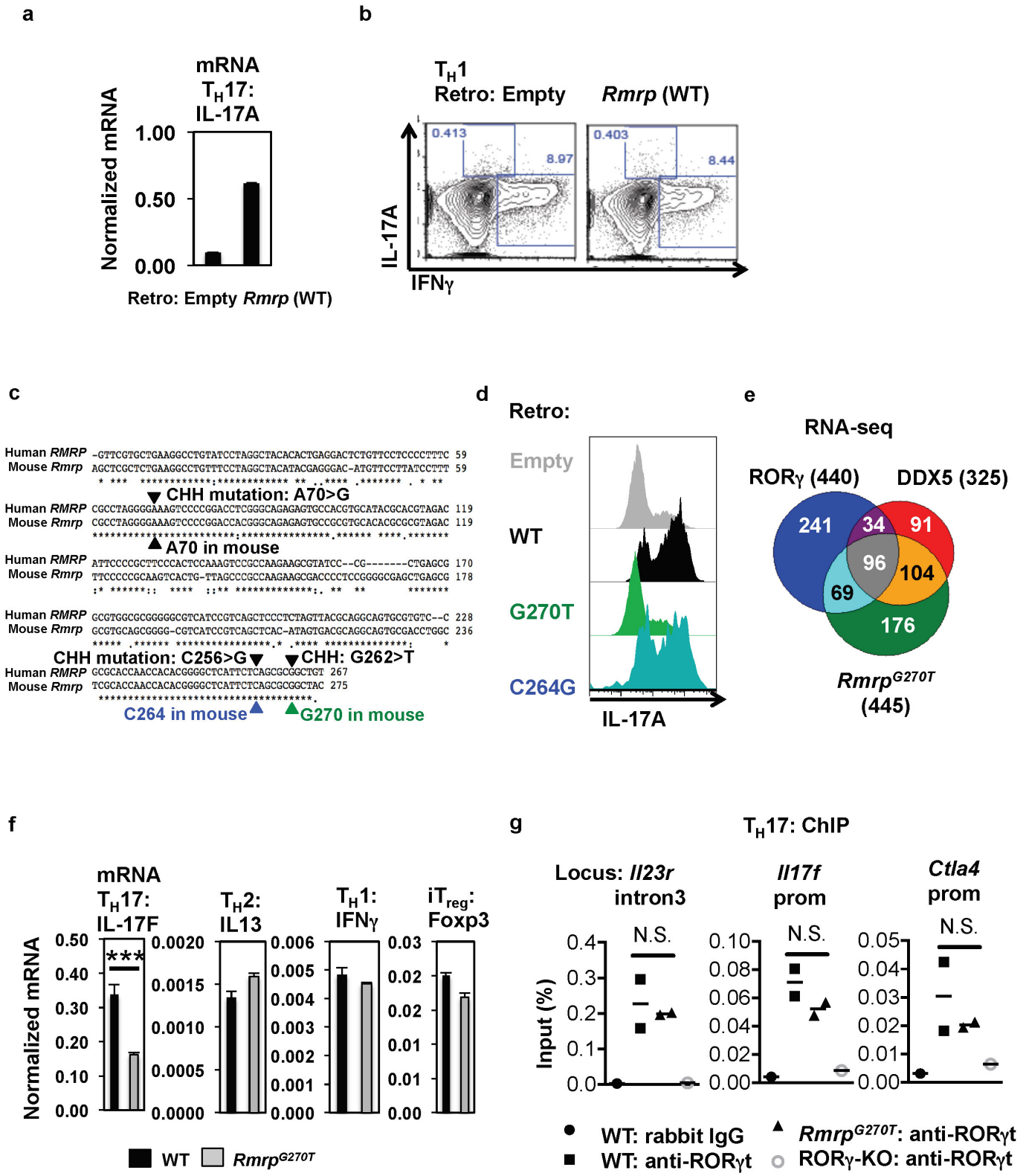

Extended Data Figure 7 | Effects of wild-type and mutant *Rmrp* in T-cell differentiation. a, *Il17a* mRNA in cell lysates of *in vitro* polarized mouse T_H17 cells at 96 h after transduction of control vector or wild-type *Rmrp*. Results are representative of two independent experiments. **b**, IFNγ production in polarized mouse T_H1 cells at 96 h after transduction of control or *Rmrp*-encoding vector. Representative of two independent experiments. Each experiment was performed with two technical replicates. **c**, Comparison of human and mouse *Rmrp* sequences. Several mutations identified in CHH patients are highlighted. **d**, IL-17A production in polarized mouse T_H17 cells at 96 h after transduction of wild-type or mutant *Rmrp* vectors. Representative of two independent experiments. **e**, Venn diagram depicting the number of distinct and overlapping genes regulated by RORγt, DDX5 and *Rmrp* in *in vitro* polarized T_H17 cells. **f**, Expression of cytokine and *Foxp3* mRNAs in T cells from wild-type or $Rmrp^{G270T/G270T}$ mice cultured *in vitro* in T_H17-, iT_{reg}-, T_H1- and T_H2-polarizing conditions. Results are representative of two independent experiments. Each experiment was performed with two technical replicates. $^{***}P < 0.001$ (unpaired, *t*-test). **g**, ChIP-qPCR experiment using anti-RORγ/γt antibodies on chromatin of T_H17 cells from wild-type or mutant mice cultured for 48 h *in vitro*. Each dot represents a different biological sample. Wild type, $n = 2$; $Rmrp^{G270T}$, $n = 2$. Results are representative of three separate independent experiments. Graphs show mean ± s.d. (unpaired, *t*-test).

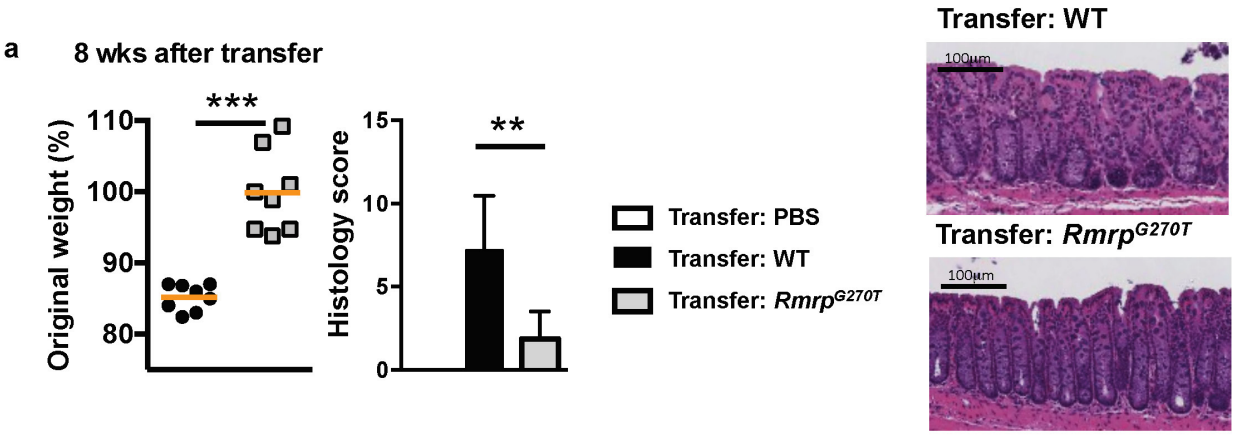

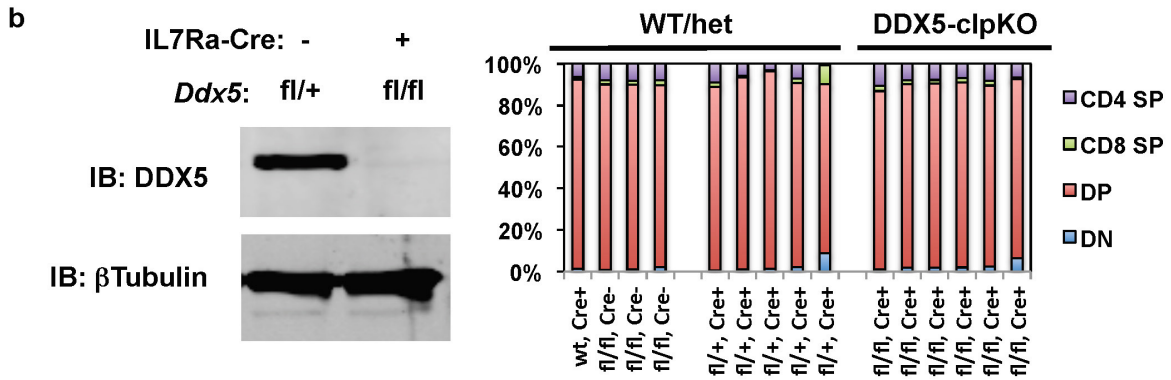

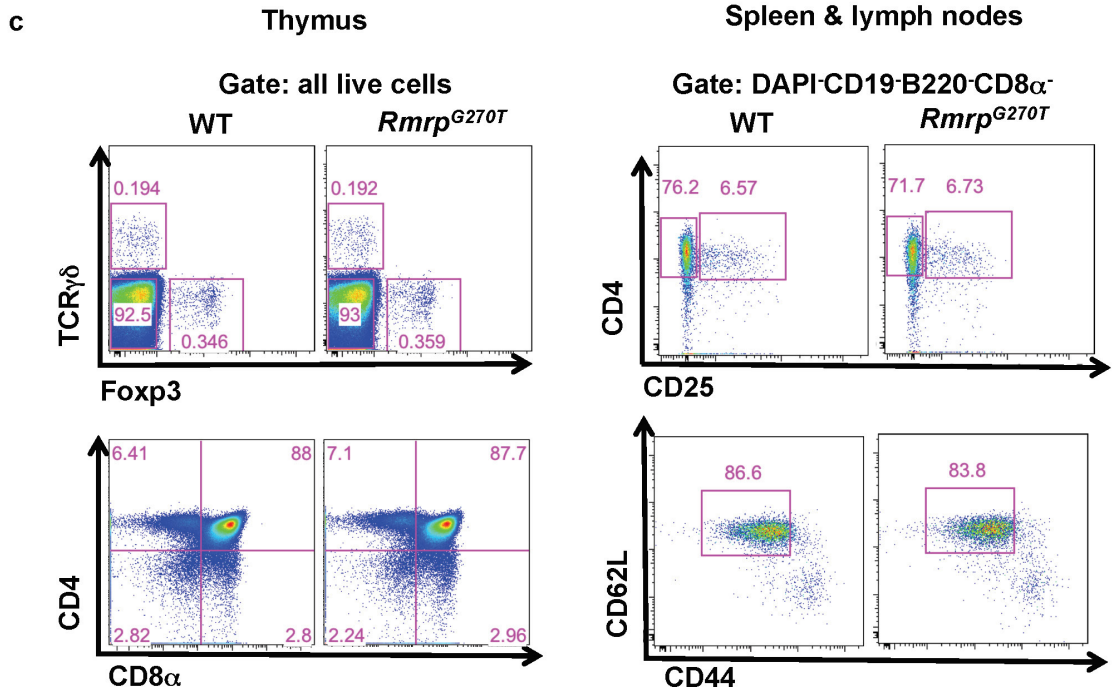

Extended Data Figure 8 | Effect of *Ddx5* and *Rmrp* mutations in inflammation and thymocyte development. a, Left, percentage weight change in $Rag2^{-/-}$ recipients of wild-type (black circles) or $Rmrp^{G270T/G270T}$ (grey squares) naive $CD4^+$ T cells in the transfer model of colitis. Animal weight was measured on day 56 (wild type, $n=8$; $Rmrp^{G270T/G270T}$, $n=8$, combined from three independent experiments). Graphs show mean ± s.d. $^{***}P<0.001$ (unpaired, *t*-test). Middle, histology score (scale of 0–24) (wild type, $n=8$; $Rmrp^{G270T/G270T}$, $n=5$), combined from two independent experiments. $^{**}P<0.01$ (unpaired, *t*-test). Right, representative H&E staining of large intestine from $Rag2^{-/-}$ mice on day 56 after naive T-cell transfer. **b**, Mice with deletion of *Ddx5* in early common lymphoid progenitors (DDX5-clpKO) have normal thymic development. Left, immunoblot of thymocyte lysates with anti-DDX5 antibody confirmed depletion of DDX5. Right, percentage of CD4 single-positive (SP), CD8α SP, double-positive (DP) and double-negative (DN) cells among total thymocytes. Each bar represents the result from one mouse (WT/het, $n=9$; DDX5-clpKO, $n=6$). For uncropped gels, see Supplementary Fig. 1. **c**, Thymocyte and peripheral T-cell surface phenotypes of wild-type and $Rmrp^{G270T/G270T}$ knock-in mice at steady state. Peripheral T-cell gate, $DAPI^-CD19^-CD8\alpha^-CD4^+$.

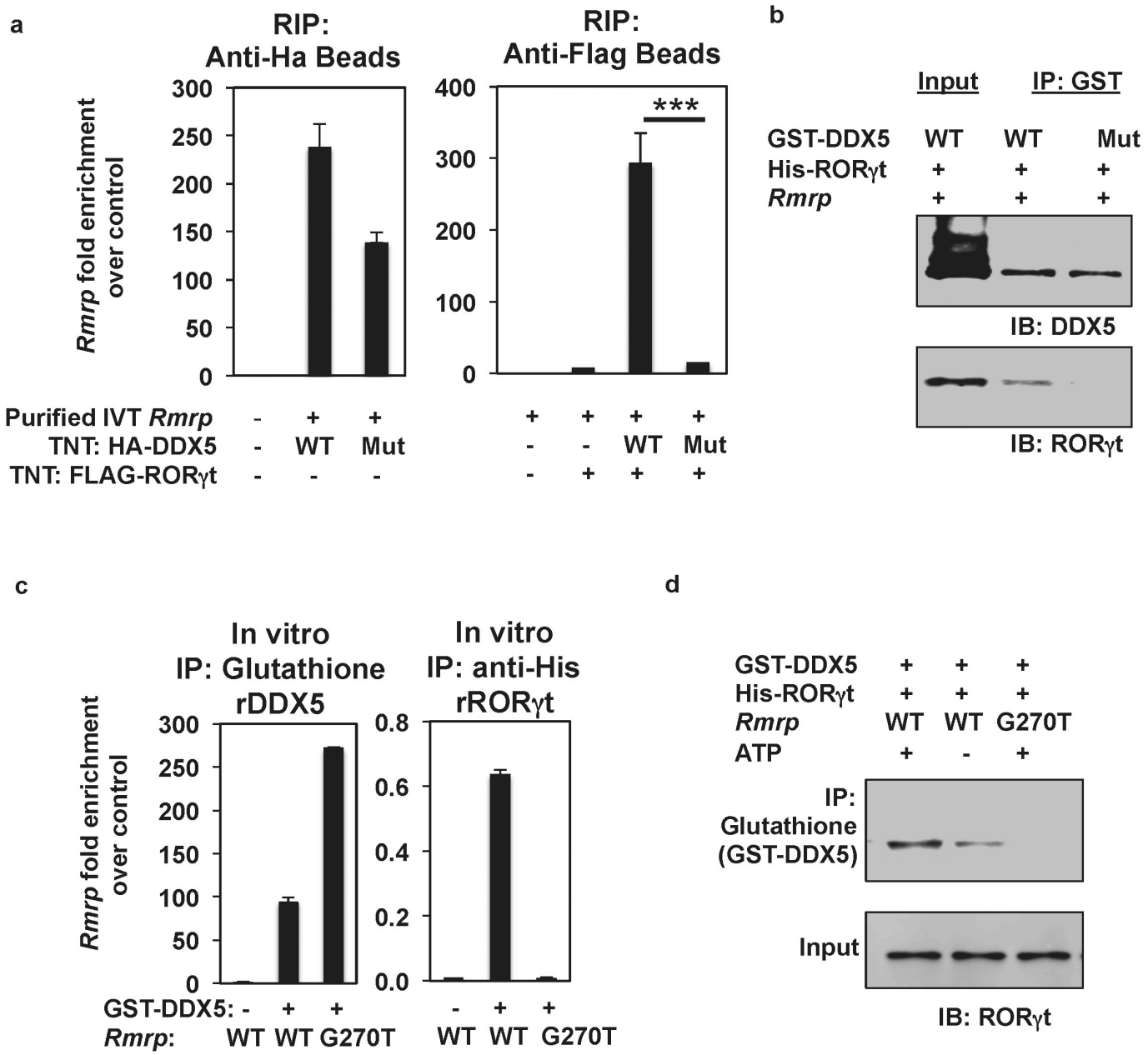

Extended Data Figure 9 | Association of *Rmrp* lncRNA with DDX5 and RORγt *in vitro*. **a**, *In vitro* translated (TNT) HA-tagged wild-type or helicase-dead DDX5 and Flag-tagged RORγt were incubated with *in vitro* transcribed *Rmrp*. After capture on anti-HA or anti-Flag beads, the amount of lncRNA was determined by RT–qPCR. Data are representative of two independent experiments, and each experiment was performed with two technical replicates. **b**, Helicase requirement for *in vitro* interaction of DDX5 and RORγt. Recombinant GST–DDX5 (wild type or helicase-dead mutant) and His–RORγt full-length protein were synthesized in *Escherichia coli*, purified, and assayed for binding with or without *in vitro* transcribed *Rmrp* RNA in the presence exogenous ATP. **c**, Association of *in vitro* transcribed wild-type and mutant *Rmrp* with recombinant GST–DDX5 captured on glutathione beads (left) or with recombinant GST–DDX5 and His–RORγt captured with anti-His antibody. Amounts of associated *Rmrp* were quantified using RT–qPCR. Data are representative of two independent experiments. Each experiment was performed with two technical replicates. **d**, Comparison of ability of *in vitro* transcribed wild-type and $Rmrp^{G270T}$ lncRNA to promote interaction between recombinant RORγt and DDX5 *in vitro*. All graphs show mean ± s.d. $***P < 0.001$ (unpaired, *t*-test). For uncropped gels, see Supplementary Fig. 1.

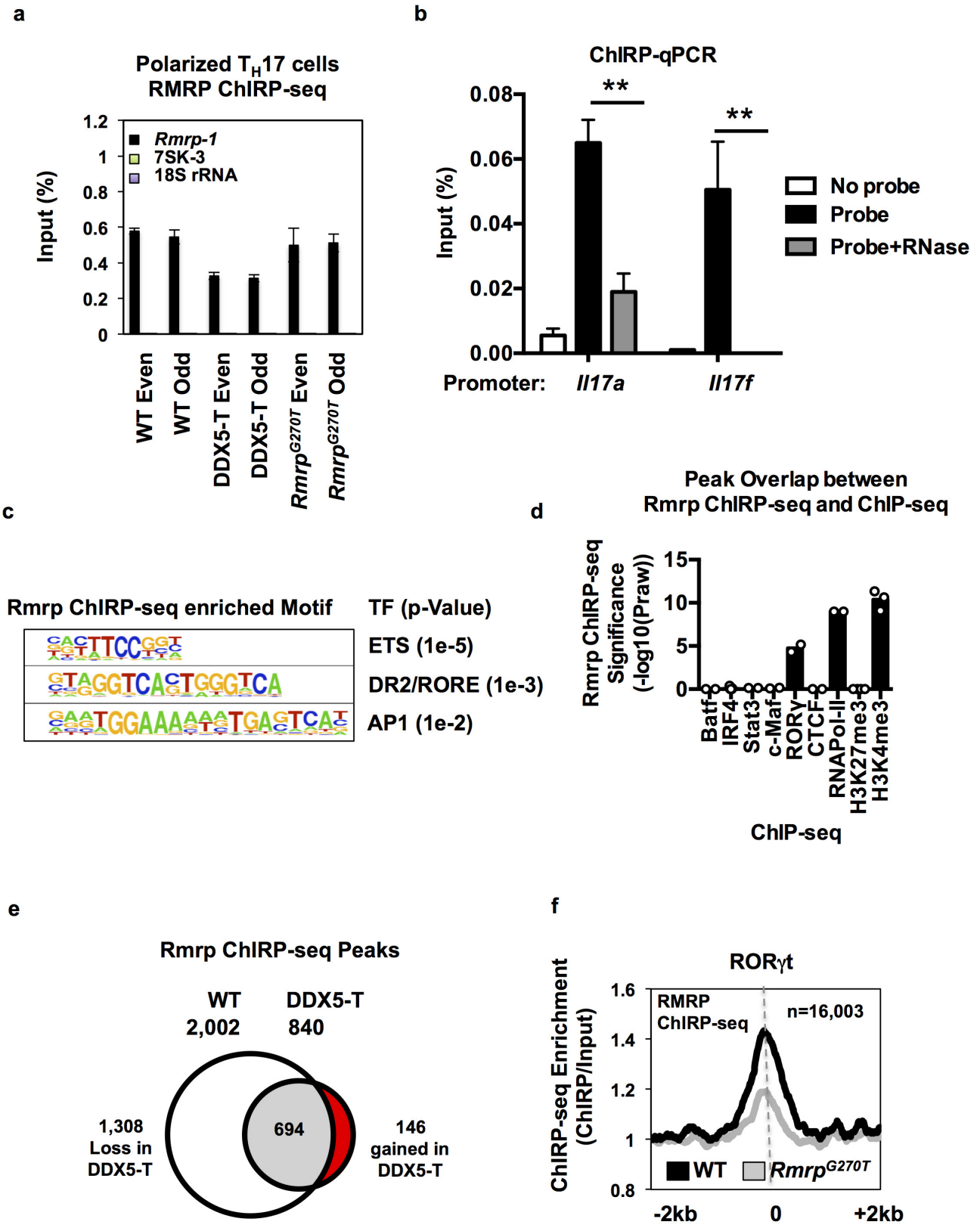

Extended Data Figure 10 | *Rmrp* chromatin localization in T_H17 cells. **a**, ChIRP-seq sample validation of *Rmrp* RNA pull-down over other nuclear noncoding RNAs using pools of 'even' or 'odd' capture probes. Graphs show mean ± s.d. **b**, ChIRP-qPCR of *Rmrp* RNA pull-down from wild-type T_H17 cell lysate treated with or without RNase ($n = 2$). qPCR for each sample was performed with two technical replicates. Graph shows mean ± s.d. $^{**}P < 0.001$ (unpaired, *t*-test). **c**, HOMER motif analysis reveals top three DNA motifs within *Rmrp*-enriched peaks. **d**, Significance of peak overlaps between *Rmrp* ChIRP-seq and ChIP-seq for BATF ($n = 2$), IRF4 ($n = 7$), STAT3 ($n = 2$), c-Maf ($n = 2$), RORγt ($n = 2$), CTCF ($n = 2$), RNA Pol II ($n = 2$), H3K27me3 ($n = 4$) and H3K4me3 ($n = 3$) in T_H17 cells (hypergeometric distribution). Each dot represents a separate biological replicate of ChIP-seq experiments. **e**, Venn diagram depicting changes in peaks called from *Rmrp* (ChIRP-seq) experiments in wild-type and DDX5-T T_H17 cells. **f**, Comparison of *Rmrp* chromatin occupancy (ChIRP-seq) at known RORγt occupied loci in *in vitro* polarized T_H17 cells from wild-type and $Rmrp^{G270T/G270T}$ mice.

CORRIGENDUM

doi:10.1038/nature16968

Corrigendum: DDX5 and its associated lncRNA Rmrp modulate TH17 cell effector functions

Wendy Huang, Benjamin Thomas, Ryan A. Flynn, Samuel J. Gavzy, Lin Wu, Sangwon V. Kim, Jason A. Hall, Emily R. Miraldi, Charles P. Ng, Frank Rigo, Sarah Meadows, Nina R. Montoya, Natalia G. Herrera, Ana I. Domingos, Fraydoon Rastinejad, Richard M. Myers, Frances V. Fuller-Pace, Richard Bonneau, Howard Y. Chang, Oreste Acuto & Dan R. Littman

Nature **528,** 517–522 (2015); doi:10.1038/nature16193

In this Article, author 'Frank Rigo' was incorrectly listed with a middle initial; this has been corrected in the online versions of the paper.